

# A Comprehensive Analysis of Fermi Gamma-Ray Burst Data with thermal and non-thermal component

## ABSTRACT

**Aims:** We have investigated the properties of thermal and non-thermal components as well as the effect of the thermal components on the overall gamma-ray burst (GRB) spectra with 20 GRBs observed by Fermi/GBM.

**Methodology:** We first comprehensively compare the fitting results of the two different models (Band Only and Band+Blackbody (BB)) in the time-resolved spectra. We then use a power-law with an exponential cutoff + Blackbody+ power law (CPL+BB+PL) model to fit the time-resolved spectra. Finally, we present the spectral evolutions between the spectral parameters and their physical significance.

**Results:** The thermal component **decreases** the low-energy index  $\alpha$  and does not seem to affect high-energy index  $\beta$ ; the thermal component makes the peak energy  $E_p$  increase and it leads to faster decay of  $E_p$  in decaying episodes. Four GRBs can be fitted by **CPL+BB+PL** model, which shows that PL component appears in the energy spectrum at the beginning of the fireball explosion.

**Conclusion:** (i) The radiation mechanisms of a **few** bursts are consistent with the synchrotron radiation while three bursts can be explained by jitter radiation; (ii) comparing the particle acceleration models in GRBs, the magnetic reconnection is more suitable to the prompt emission than the internal shock; (iii) the correlation between spectral peak energy  $E_p$  and thermal temperature  $kT$  shows that there are magnetically-dominant jets in the GRBs; (IV) the  $E_p-F_p$  (**energy flux**) relation is weaker in Band+BB, which may be regarded as one of the evidences of the existence of the thermal radiation in GRB prompt emission.

*Keywords: Gamma-ray bursts: general – methods: statistical – radiation mechanisms: thermal components non-thermal components*

## INTRODUCTION

Gamma-ray bursts (GRBs) are the most energetic explosions at cosmological distances (Meegan et al. 1992; Bhat & Guiriec 2011). It is most likely caused by the result of cataclysmic events such as the collapse of a massive star (Woosley 1993; MacFadyen & Woosley 1999) or the merger of two dense objects (Paczynski 1986; Fryer et al. 1999; Rosswog 2003). **Though these two mechanisms are truly widely accepted in the field of GRBs, it should also be noted that the possibility that a small portion of GRBs might be produced by other mechanisms still could not be expelled. For example, some special GRBs might also be produced by strange quark stars (e. g. Dai & Lu T., (1998); Geng J., et al., 2021).**

While various observations and theory studies have been carried out over 50 years after the discovery of the GRB, there are still many unresolved problems in the prompt emission phase. The prompt emission mechanism of GRBs is one of the unresolved issues. Regardless of the nature and formation mechanism of the GRB central engine, the fireball model is still the most popular theoretical model in GRBs. Internal-external-shock model can explain the prompt emission and afterglow based on the fireball model. (Tavani 1996; Zhang & Mészáros 2004; Mészáros and Rees 1993; 1997; Sari et al. 1998). Some evidences

showed Poynting-flux-dominated outflow model could provide a viable mechanism for generating the observed prompt emission (e.g., Giannios 2009; Zhang & Yan 2011). Moreover, the fireball model also predicts strong thermal emission emanating from the jet's photosphere (Paczynski 1986; Goodman 1986; Zhang 2014).

Analysis of the prompt emission spectroscopy can provide us valuable clues to understand prompt emission mechanism. The empirical Band function (Band et al. 1993), has traditionally been fitted to provide a good description of the prompt emission spectra. However, many studies revealed that the single Band function cannot well interpret the spectra of entire GRBs. For example, Ryde et al. (2014) showed the spectra is thermal (blackbody (BB)) at the beginning and later becomes non-thermal. Since then, many studies showed that GRB spectra are composed of two components, thermal and non-thermal component even three components. These components can be BB, Band or a power-law with an exponential cutoff (hereafter CPL). In addition, there may be a power-law component in some GRBs (e.g. Ackermann et al. 2010; Guiriec et al. 2011, 2013, 2015a, 2015b; Ryde 2005; Pe'er & Ryde 2009).

Spectral evolution of GRBs is a common phenomenon. The peak energy  $E_p$  of  $\nu F_\nu$  spectra decays with time,  $E_p \propto t^{-\delta}$ , during the decay pulse (Crider et al. 1997; Daigne & Mochkovitch 2003; Peng et al. 2009). In addition, the thermal energy  $kT$  of BB spectra also decay with time following almost the same  $\delta$  (Pe'er 2008; Ryde & Pe'er 2009). Previous studies have shown that  $E_p$  is positively correlated with low-energy power-law index  $\alpha$ ,  $E_p \propto T^\alpha$ , (Burgess et al. 2014a) and the same correlation  $kT \propto t^{-\alpha}$  also exists (Pe'er 2008; Ryde & Pe'er 2009).

Some studies analyzed some single bursts including a significant thermal spectral contribution to check the effects of the thermal components on the non-thermal components as well as hardness-luminosity relation (Guiriec et al. 2011, 2013, 2015a, 2015b). For example, Huang et al. (2016) performed a detail analysis of the spectra of GRB100724B which is dominated by the empirical Band function form, including a significant thermal spectral contribution (Guiriec et al. 2011). However, they focus their attentions on the single burst. In this paper we would like to comprehensively study 20 bursts with thermal and non-thermal components to investigate how the thermal component simultaneously may affect the non-thermal component, the whole shape and evolution of the spectra, and we compare our results with previous studies. In sections 2 and 3 we describe the sample selection and the analysis methods. We present our fitting results in section 4. Discussion and conclusions are given in section 5. We have adopted the cosmological constant  $H_0 = 70 \text{ km s}^{-1} \text{ Mpc}^{-1}$ ,  $\Omega_m = 0.3$ .

## METHODOLOGY

### 1. THE SAMPLE SELECTION AND DATA ANALYSIS

The Fermi satellite was launched in 2008 which is composed of Gamma-ray Burst Monitor (GBM) and Large Areas Telescope. To study the spectral components and evolutions from keV to MeV Band, we select the GRB data detected by Fermi GBM from 1 January 2012 to 1 July 2016 in FSSC (Fermi Science Support Center), which converges an energy range from 8 keV to 40 MeV (Meegan et al. 2009). We adopt the TTE file, which is one of the GBM spectral files and has the finest time (2  $\mu\text{s}$ ) and energy evolution for the purpose of the time-resolved analysis in the prompt emission spectra. In the other hand, the bursts which we selected should be bright and have a sufficiently high ratio of signal-to-noise. Therefore, these bright bursts satisfy the same criteria as Yu et al. (2016): the energy flux  $F_p \geq 4 \times 10^{-5} \text{ erg s}^{-1} \text{ cm}^{-2}$  and the peak photon flux  $F_\nu \geq 20 \text{ photons s}^{-1} \text{ cm}^{-2}$ . We exclude some bursts that

the  $T_{90}$  are greater than 300 s because the TTE data are available from 30 s before triggers to 300 s after triggers. In this way there are 67 bursts meeting the criteria. For each burst, we select NaI and BGO detectors according to the quicklook.pdf file. Besides, the energy ranges of NaI and BGO are from 8 keV to 900 keV and from 250 keV to 40 MeV, respectively. Moreover, it is necessary to perform the background fitting before the spectral analysis, and the background was fitted with a polynomial function with order 2-4 through two background intervals before and after the emission pulses. The data were fitted by Rmfit 4.3.2 package and the minimizing statistics in the fitting is the Cash C-Statistics (Cash 1979, hereafter C-stat), which is a likelihood technique converging to a  $\chi^2$  for a specific data set when there are enough counts (Guiriec et al. 2015b).

**Table 1 The sample bursts with their duration and detector**

GRB	$T_{90}$ / s	NaI	BGO
120129A	3.072	n7 n8 nb	b1
120707A	40.960	n6 n9 nb	b1
121225B	58.497	n1 n3 n5	b0
130305A	25.600	n6 n9 na	b1
130502B	24.320	n6 n7 n8	b1
130504C	73.217	n6 n9 na	b1
130518A	48.577	n0 n3 n4	b0
130606B	52.225	n7 n8 n11	b1
131231A	31.232	n0 n3 n4	b0
140206A	146.690	n0 n1 n3	b0
140329A	21.504	n7 n8 nb	b1
140523A	19.200	n0 n3 n4	b0
150201A	15.616	n0 n3 n4	b0
150314A	10.688	n9 na	b1
150403A	22.272	n3 n4	b0
150627A	64.577	n3 n4	b0
150902A	13.568	n0 n1 n3	b0
151227B	43.008	n1 n2 n5	b0
151231A	71.425	n8 nb	b1
160422A	12.288	n0 n1 n3	b0

Table 2 Time-integrated spectrum fitting results for 20 bursts

GRB	model	Band/CPL			BB	CPL/PL		$F_p / \text{erg s}^{-1} \text{cm}^{-2}$	C-stat/DOF
		$E_{\text{peak}}/\text{keV}$	$\alpha$	$\beta$	kT/keV	$E_{\text{peak}}/\text{keV}$	$p$		
120129A	Band	276.8±6.81	-0.75±0.02	-2.46±0.06				6.75e-6±4.80e-8	853/481
	Band+BB	290.6±8.90	-0.62±0.04	-2.54±0.08	11.41±0.65			6.79e-6±5.00e-8	789/479
	Band+PL	291.6±9.34	-0.78±0.05	-2.52±0.13			-1.73	6.82e-6±2.70e-7	857/479
	CPL+BB+PL	366.0±13.80	-0.81±0.06		18.73±1.21		-1.36±1.85	6.97e-6±6.20e-8	815/478
120707A	Band	123.60±6.54	-0.89±0.05	-2.12±0.03				1.42e-6±1.30e-8	1492/360
	Band+BB	132.50±9.72	-0.47±0.23	-2.15±0.03	7.76±0.55			1.41e-6±1.30e-8	1467/358
	Band+PL	141.00±6.93	-0.98±0.04	-2.26±0.05			0.09±0.51	1.38e-6±1.60e-8	1449/358
121225B	Band	307.40±15.20	-1.15±0.01	-2.13±0.62				8.50e-7±8.40e-9	911/504
	Band+BB	667.10±99.80	-1.36±0.03	-2.43±0.22	32.69±1.42			8.73e-7±1.10e-8	876/502
	Band+PL	242.40±21.70	-0.88±0.23	-2.05±0.05			-0.98±1.25	8.41e-7±8.20e-9	888/502
	CPL+BB+PL	707.7±104.00	-1.37±0.02		38.53±4.73			8.76e-7±9.90e-9	870/501
130502B	Band	286.20±4.45	-0.60±0.01	-2.45±0.05				2.76e-6±1.70e-8	1001/483
	Band+BB	333.90±13.00	-0.68±0.02	-2.62±0.08	27.67±2.21			2.76e-6±1.70e-8	983/481
	CPL+PL	310.3±5.87	-0.63±0.03				-1.25±0.18	2.71e-6±1.80e-8	1098/482
	CPL+BB+PL	378.00±12.50	-0.74±0.03		29.88±1.42		-1.21±0.38	2.79e-6±2.80e-8	1008/480
130305A	Band	549.40±20.70	-0.51±0.02	-2.28±0.08				1.74e-6±2.10e-8	1060/501
	Band+BB	694.90±51.50	-0.58±0.04	-2.45±0.12	38.53±4.73			1.77e-6±2.30e-8	1040/499
130504C	Band+CPL	396.50±88.50	-0.40±0.07	-2.14±0.12		731.40±70.90	4.87±5.89	1.78e-6±2.40e-8	1046/498
	Band	549.70±10.00	-1.20±0.01	-2.19±0.07				1.15e-6±1.00e-8	1781/482
	Band+BB	460.90±27.30	-1.05±0.03	-2.16±0.06	7.48±0.39			1.15e-6±1.00e-8	1744/480
	Band+PL	546.30±55.00	-1.19±0.08	-2.20±0.27			-1.78±5.43	1.15e-6±1.10e-8	1782/480
130518A	Band	390.30±12.00	-0.88±0.01	-2.34±0.07				1.32e-6±1.00e-8	790/484
	Band+BB	547.90±35.70	-1.00±0.03	-2.69±0.19	34.73±2.55			1.36e-6±1.30e-8	763/482
	Band+CPL	1433±604	-0.79±1.38	< 5		257.70±47.30	-0.82±0.19	1.34e-6±1.40e-8	756/481
130606B	Band	424.30±11.10	-1.18±0.01	-2.04±0.02				2.54e-6±1.00e-8	1990/481
	Band+BB	413.00±12.50	-1.08±0.02	-2.05±0.02	9.18±0.32			2.55e-6±1.00e-8	1839/479
	CPL+PL	473.10±15.10	-1.18±0.03				-1.44±0.08	2.60e-6±1.10e-8	2150/480
	Band+PL	431.00±21.30	-1.18±0.04	-2.05±0.06			-1.59±48.70	2.55e-6±2.40e-8	1991/479
131231198	Band	192.60±3.67	-1.25±0.01	-2.39±0.04				2.24e-6±9.30e-9	1630/484
	Band+BB	201.30±4.54	-1.17±0.02	-2.44±0.04	7.36±0.30			2.24e-6±9.40e-9	1514/482
140206A	Band	327.8±14.70	-1.23±0.01	-1.99±0.03				7.85e-7±9.40e-9	4044/484
	Band+BB	622.2±106.00	-1.41±0.02	-1.93±0.04	37.04±1.37			7.77e-7±6.80e-9	3967/482
	Band+PL	240.10±14.70	-1.01±0.07	-1.94±0.02			-3.17±0.49	7.78e-7±4.70e-9	3941/482
	CPL+BB+PL	348.00±35.20	-0.89±0.15		31.44±2.64		-1.64±0.02	7.73e-7±7.60e-9	3947/481
140329A	Band	218.50±6.12	-0.80±0.02	-2.20±0.03				1.93e-6±1.40e-8	971/360
	Band+BB	246.80±8.81	-0.68±0.04	-2.30±0.05	11.00±0.59			1.94e-6±1.50e-8	894/358
	CPL+BB+PL	351.90±14.20	-0.92±0.08		17.64±0.83		-1.45±0.75	1.99e-6±1.90e-8	956/357
140523A	Band	265.80±7.93	-1.08±0.01	-2.78±0.18				1.65e-6±1.40e-8	851/484
	Band+BB	269.00±9.25	-0.99±0.03	-2.82±0.19	8.64±0.68			1.65e-6±1.40e-8	824/482
	CPL+BB+PL	268.50±10.20	-0.93±0.12		9.05±0.84		-1.63±0.20	1.64e-6±1.70e-8	827/481
150201A	Band	120.80±2.04	-0.95±0.02	-2.54±0.04				1.92e-6±1.30e-8	917/484
	Band+BB	131.70±3.30	-0.90±0.03	-2.62±0.05	8.32±0.61			1.92e-6±1.30e-8	869/482
	Band+PL	121.90±2.11	-0.96±0.01	-2.60±0.55			-0.83±1.77	1.91e-6±1.70e-8	912/482
	CPL+BB+PL	137.10±2.89	-0.79±0.14		9.41±0.47		-1.66±0.10	1.85e-6±1.20e-8	894/481
150314A	Band	366.20±7.29	-0.73±0.01	-2.75±0.11				4.90e-6±3.50e-8	725/359
	Band+BB	447.40±15.80	-0.81±0.02	-3.43±0.44	29.38±2.06			5.01e-6±4.40e-8	681/357
	Band+PL	365.30±7.54	-0.73±0.01	-2.76±0.12			-0.15±13.90	4.89e-6±3.70e-8	725/357
150403A	Band	280.20±9.33	-0.49±0.03	-1.99±0.03				1.51e-6±1.30e-8	708/362
	Band+BB	553.00±33.80	-0.70±0.03	-2.39±0.10	24.86±1.12			1.60e-6±1.90e-8	625/360
	Band+CPL	671.30±61.10	-0.27±1.57	-2.50±0.14		127.10±31.50	-0.14±0.45	1.62e-6±1.90e-8	597/359
150627A	Band	238.60±4.71	-1.01±0.01	-2.60±0.03				2.17e-6±1.00e-8	1377/362
	Band+BB	241.60±5.85	-0.92±0.02	-2.23±0.03	8.34±0.43			2.18e-6±1.10e-8	1307/360
	Band+PL	224.40±7.28	-1.02±0.04	-2.22±0.06			-1.68±137	2.17e-6±1.40e-8	1427/360
	CPL+BB+PL	355.50±13.90	-1.14±0.04		21.45±1.00		-1.45±0.35	2.23e-6±1.40e-8	1427/359

GRB	model	Band/CPL			BB	CPL/PL		$F_p / \text{erg s}^{-1} \text{cm}^{-2}$	C-stat/DOF
		$E_{\text{peak}}/\text{keV}$	$\alpha$	$\beta$	kT/keV	$E_{\text{peak}}/\text{keV}$	$p$		
150902A	Band	383.30±7.98	-0.66±0.15	-2.32±0.04				2.86e-6±1.80e-8	939/483
	Band+BB	478.60±19.70	-0.74±0.02	-2.53±0.08	30.36±2.32			2.92e-6±2.20e-8	909/482
	Band+PL	396.50±13.00	-0.68±0.04	-2.36±0.10			-1.2	2.87e-6±1.50e-8	941/482
151227B	Band+CPL	668.8±520.00	-0.48±3.49	-2.63±0.17		196.20±75.90	-0.56±0.76	2.93e-6±2.30e-8	900/481
	Band	256.50±17.10	-1.21±0.02	-2.08±0.06				8.46e-7±8.70e-9	1025/503
	Band+BB	243.50±18.30	-1.01±0.06	-2.09±0.06	7.37±0.44			8.47e-7±8.90e-8	982/502
151231A	CPL+BB+PL	292.80±26.80	-1.07±0.16		8.42±0.58		-1.49±0.28	8.41e-7±1.30e-8	994/501
	Band	185.40±8.22		-2.14±0.07				9.96e-7±1.10e-8	591/360
	Band+BB	178.20±10.20	-0.35±0.28	-2.41±0.06				9.91e-7±1.10e-8	579/358
160422A	Band+PL	186.70±10.90	-0.90±0.09	-2.48±0.24			-1.38±4.59	9.95e-7±1.10e-8	591/358
	CPL+BB+PL	245.30±18.50	-1.05±0.22		25.59±3.33		-1.61±0.15	9.58e-7±1.10e-8	604/357
	Band	265.70±6.22	-1.17±0.01	-2.56±0.09				2.34e-6±1.50e-8	1057/484
160422A	Band+BB	275.40±8.03	-1.15±0.01	-2.63±0.11	9.79±1.35			2.35e-6±1.50e-8	1043/482
	Band+PL	266.70±12.00	-1.17±0.06	-2.57±0.16			-1.48±0.64	2.34e-6±1.60e-8	1057/482
	CPL+BB+PL	290.20±11.90	-1.17±0.05		11.31±1.39		-1.48±0.64	2.36e-6±1.80e-8	1048/481

UNDER PEER REVIEW

## 2. THE ANALYSIS METHOD AND FITTING MODEL

The purpose of this paper is to investigate the simultaneous effect of the thermal component on the non-thermal component and the spectral evolution in whole prompt emission. Therefore, we should make sure the thermal component exists in the prompt emission spectra at first. We perform the time-integrated analysis in the main part of the prompt emission with the empirical Band function, and simultaneously fit the same data with a combination of Band and each of functions as follows: *BB*, *PL* and *CPL*. When we add new component to Band, the C-stat value will decrease obviously, especially in Band+BB. Moreover, the values of C-stat are obtained in the two models. To distinguish which model is suitable for the spectra, we compare the decreasing C-stat per *DOF* ( $\Delta$ C-stat) in the two model, and the Band+BB model get a better  $\Delta$ C-stat. For the fitting of time-integrated spectrum, the variation range of the C-stat value is around 100. If the statistic value of the Band+BB fitting result decreases to 100 compared with that of the Band model alone, it proves that there is thermal component during the eruption. The overall C-stat values of the time-integrated spectrum fitting results are generally several tens decrease after adding the thermal component BB. On the other hand, when Band+CPL and Band+BB are fitted, the reduced values are not much different than those of the Band function fitting alone, and sometimes Band+CPL reduces more C-stat value, so the unit degree of freedom C-stat/DOF is more appropriate. For example, in GRB150403A, compared with the fitting results of Band function alone, the overall C-stat value is reduced by 83 when Band+BB is fitted, and C-stat/DOF is 41.5; the reduced value when fitted by Band+CPL is 111, while the C-stat/DOF is 37. We remove some bursts due to the lack of thermal component in the prompt emission time-integrated spectra. Finally, we obtain 20 GRBs and presented that in Table 1. The time-integrated fitting results are shown in Table 2. There are four empirical functions in our spectral fitting, which are listed as follows:

The Band model is defined as

$$f_{\text{band}}(E) = A \begin{cases} \left(\frac{E}{100\text{keV}}\right)^\alpha \exp\left(-\frac{(\alpha+2)E}{E_p}\right), & E < \frac{(\alpha-\beta)E_p}{(\alpha+2)} \\ \left(\frac{E}{100\text{keV}}\right)^\beta \exp(\beta-\alpha) \frac{(\alpha-\beta)E_p^{\alpha-\beta}}{100\text{keV}(\alpha+2)}, & E \geq \frac{(\alpha-\beta)E_p}{(\alpha+2)} \end{cases}$$

where  $A$  is the normalization factor at  $100\text{keV}$  in units of  $\text{phs cm}^{-2}\text{keV}^{-1}$ ;  $\alpha$  and  $\beta$  are the low-energy and high-energy power-law (PL) index, respectively;  $E_p$  is the peak energy in units of  $\text{keV}$ .

The BB model is defined as (i.e. Planck function)

$$f_{\text{BB}}(E) = A \frac{\left(\frac{E}{\text{keV}}\right)^2}{\exp\left(\frac{E}{kT}\right) - 1}$$

where  $A$  is the normalization factor at  $1\text{keV}$ ;  $kT$  is the blackbody temperature in units of  $\text{keV}$ .

The CPL is defined as

$$f_{\text{CPL}}(E) = A \left(\frac{E}{100\text{keV}}\right)^\alpha \exp\left(-\frac{(\alpha+2)E}{E_p}\right)$$

where  $A$  is the normalization factor at 100 keV in units of  $\text{phs cm}^{-2} \text{keV}^{-1}$ ;  $\alpha$  is the lower-energy power-law index;  $E_p$  is the peak energy in units of keV.

The PL model is defined as

$$f_{\text{PL}}(E) = A \left( \frac{E}{100 \text{keV}} \right)^p$$

where  $A$  is the normalization factor at 100 keV;  $p$  is the power law index.

## MULTI-COMPONENT MODEL FITTING RESULTS

We first fit the time-integrated spectra of our sample with two-component model which is a combination of Band and each of *CPL*, *BB* and *PL*, and a new multi-component model *CPL+BB+PL*, which has been presented in Guiriec et al. (2015a). We must point out that the thermal component can be modeled in time-resolved spectra in most of bursts we selected, and Burgess et al. (2014a) showed that the important information of the spectra will be covered in the time-integrated spectra.

In Table 2 the parameters of Band function surround the characteristic value, the low-energy power-law index  $\alpha \sim -1$ , the high-energy power-law index  $\beta \sim -2.2$ , the results are very consistent with Preece et al. (1998). When we add BB into Band,  $\alpha$  becomes softer,  $\beta$  is slightly smaller and  $E_p$  increases significantly in individual burst. Additionally, the peak flux of  $\nu F_{\nu}$  spectra  $F_p$  is same in all fitting model. Comparing the fitting results of Band+BB with *CPL+BB+PL*, the parameters of the two models are similar and the index of PL component of *CPL+BB+PL* model is closed to -1.5.

### Band and Band+BB model

In time-resolved analysis, we have shown the distributions of the three parameters in Figure 1 and the red curves in which are the Gaussian fit lines. And we also present the Gaussian fit results in Table 3. For some individual bursts, for example GRB150314205, GRB130606497, GRB131231198, GRB120707800,  $\alpha$  decreases when add BB into Band, but in a few time intervals it increases. It will decrease after the first rising and there seems a linear correlation in the decays of  $\alpha$  (see Figure 2). For the overall sample, the  $\alpha$  of the Band+BB spectra is softer than that of Band only (see, Table 3, Figures 1 and 2).

**Table 3 Gauss fitting results of frequency distribution statistics of each parameter in different model**

Model	parameter	$x_c$	$r^2$
Band	$\alpha$	$-0.75 \pm 0.01$	0.9541
	$\beta$	$-2.42 \pm 0.01$	0.9499
	$E_p / \text{keV}$	$208.38 \pm 8.54$	0.9603
Band+BB	$\alpha$	$-0.87 \pm 0.01$	0.9905
	$\beta$	$-2.57 \pm 0.02$	0.9216
	$E_p / \text{keV}$	$278.97 \pm 7.55$	0.9231

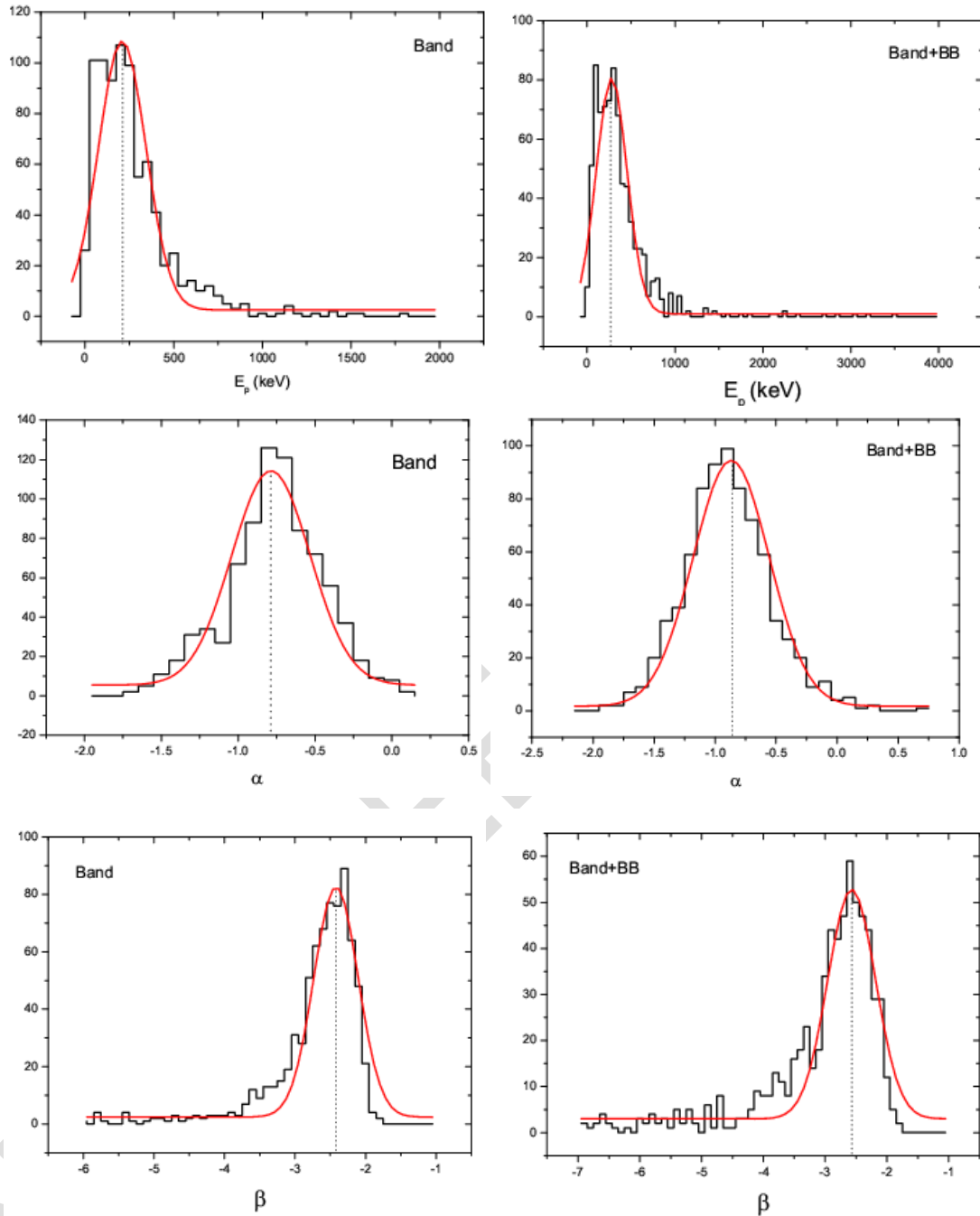


**Fig. 1** The distributions of spectral parameters in different models, and the red solid line are Gaussian fitting curve. Left panels: Band models. Right panels: Band+BB models.

The mean value of  $\beta$  is slightly smaller in Band+BB than that in Band, and it will suddenly shift to a small value ( $<5$ ) in several time intervals. Besides, the evolution with time is similar in the two models (for example GRB120129A and GRB150627A, see Figure 3).

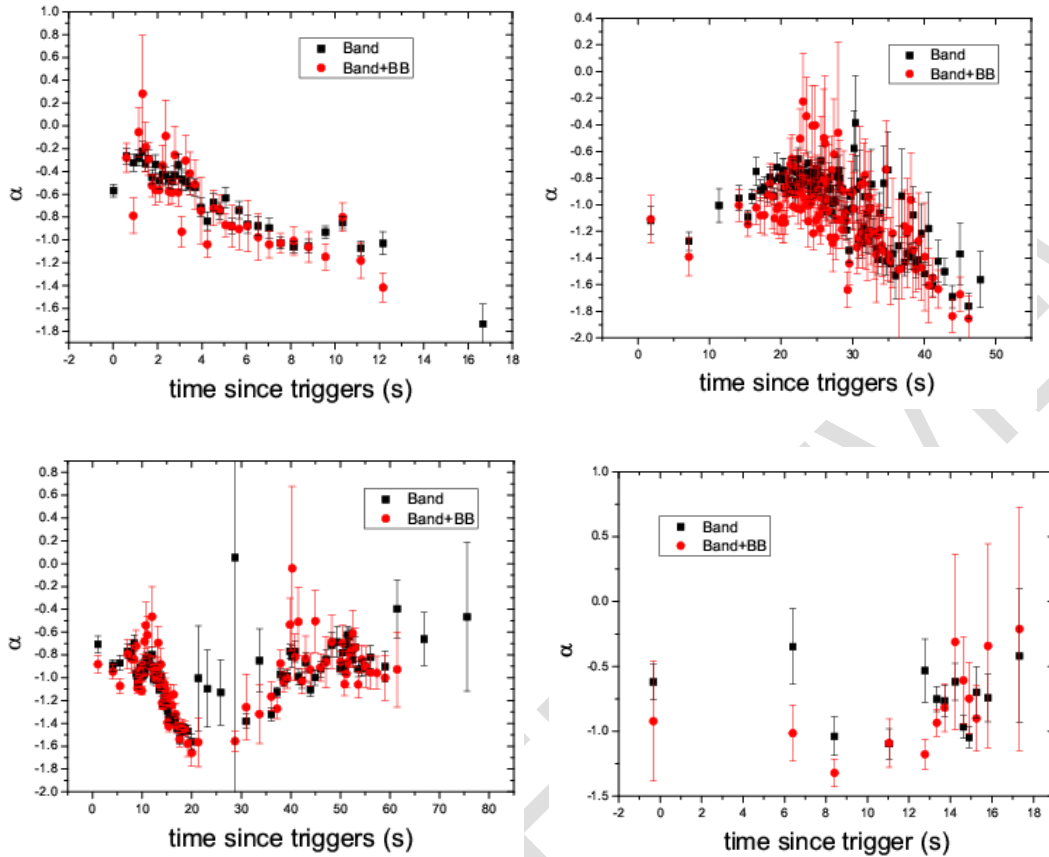


**Fig. 2** A example plot of  $\alpha$  evolution with time of the parameters in two different fitting models. Band only: the *black squares*; Band+BB: filled *red circle*; Top left : GRB150314A, Bottom left : GRB130606B, Top right : GRB131231A, Bottom right : GRB120707A.

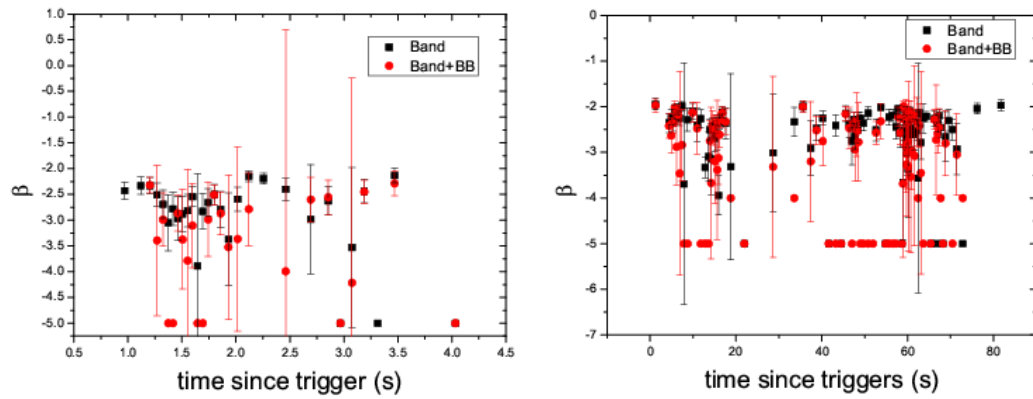


**Fig. 3** A example plot of  $\beta$  evolution with time of the parameters in two different models. Band only: the *black squares*; Band+BB: filled *red circle*. Left panel : GRB120129A, right panel : GRB150627A.

The peak energy  $E_p$  increases significantly after adding BB to Band function and the decay of  $E_p$  is faster than Band+BB (see Figure 4) due to the thermal component (Huang et al. 2016). Besides,  $F_p$  is similar in the two model (see, Figure 5). These results are very consistent with previous research (e.g. Huang et al. 2016).

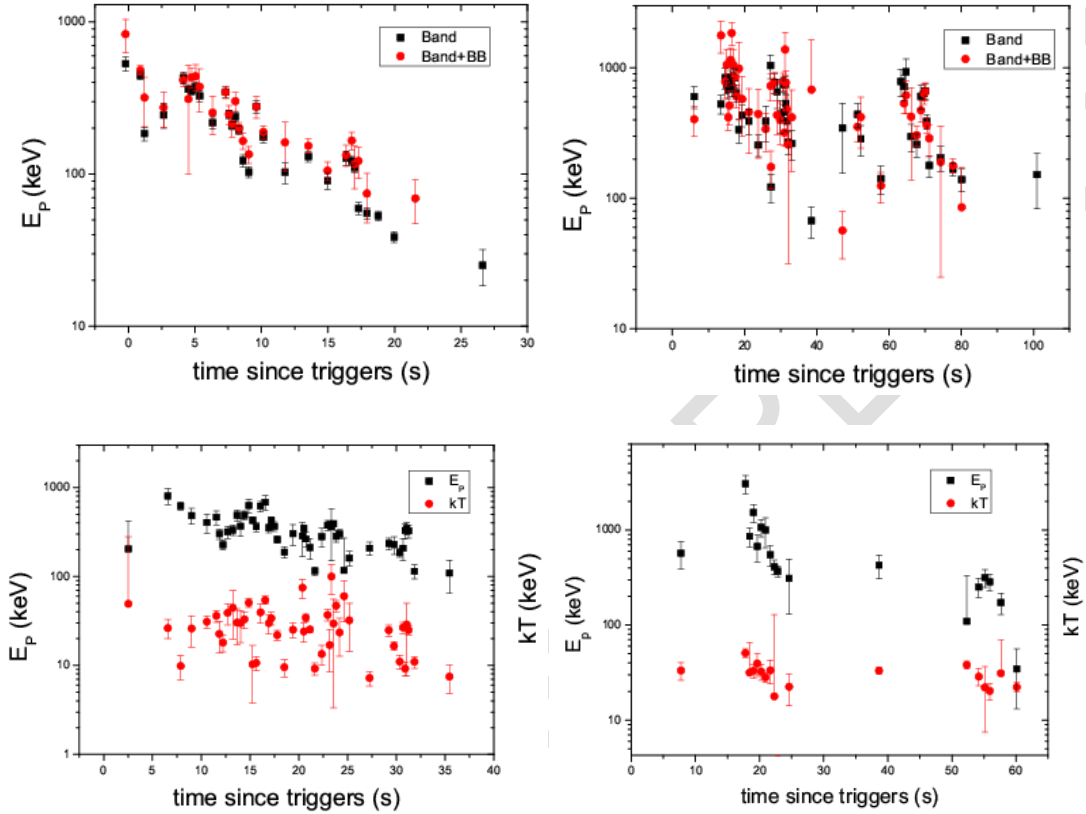
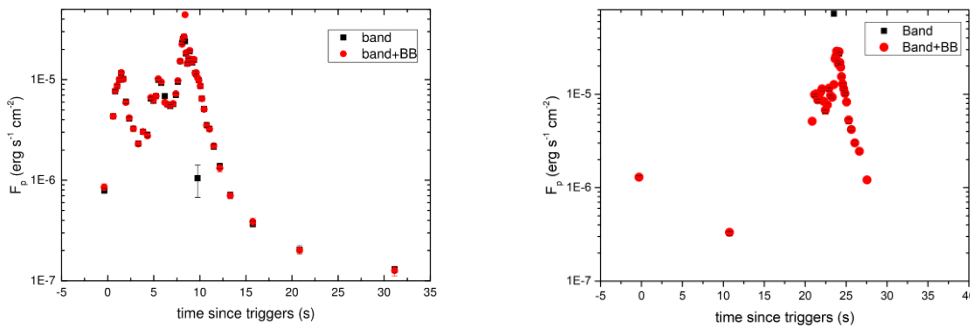
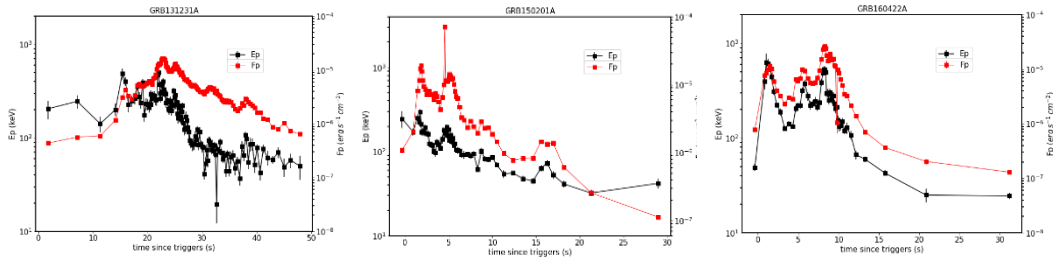


Fig. 4 A example plot of the  $E_p$  evolution with time and the thermal temperature  $kT$  fitting with Band+BB;  $E_p$ : the black squares;  $kT$ : filled red circle. Top left: GRB140523A, Bottom left: GRB130502B, Top right: GRB130504C, Bottom right: GRB121225B.



**Fig. 5** A example plot of the  $F_p$  evolution with time in two different fitting models. Band only: the *black squares*; Band+BB: the *red circle*. Left panel : GRB160422A, right panel : GRB140329A.



**Fig. 6** A example plot of the evolution with time of the peak energy  $E_p$  and the energy flux  $F_p$  fitting with Band+BB;  $E_p$ : the *black squares*;  $F_p$ : filled *red squares*. Left panel : GRB131231A ; middle panel : GRB150201A ; down panel : GRB160422A.

Previous study showed that there is a positive correlation between peak energy  $E_p$  and  $\alpha$  and the decay of peak energy  $E_p$  follows a relation with time,  $E_p \propto t^{-\delta}$ , during the decay pulse (Crider et al. 1997; Daigne & Mochkovitch 2003; Peng et al. 2009). In this work the same evolution trend has been found between  $E_p$  and peak flux  $F_p$ . Compared the evolution process of the two parameters, there are two types of evolutionary form, “Hard-to-Soft” and “Tracking”. If the evolution of  $E_p$  follows the evolution of  $F_p$ , then the evolution of  $E_p$  takes on the form of “Tracking”, such as GRB160422A (see, Figure 6); if the evolution of  $E_p$  exhibits a maximum value at the beginning of the explosion and then decays over time, the evolution of  $E_p$  at this case is inconsistent with the evolution of  $F_p$ , showing the form of “hard to soft”, such as GRB140523A (see, Figure 4); but in our fitting results, we notice that in GRB150201A (see, Figure 6), the evolution of  $E_p$  follows the form of “hard to soft” in the rise phase, but the form of “Tracking” appears in the attenuation process.

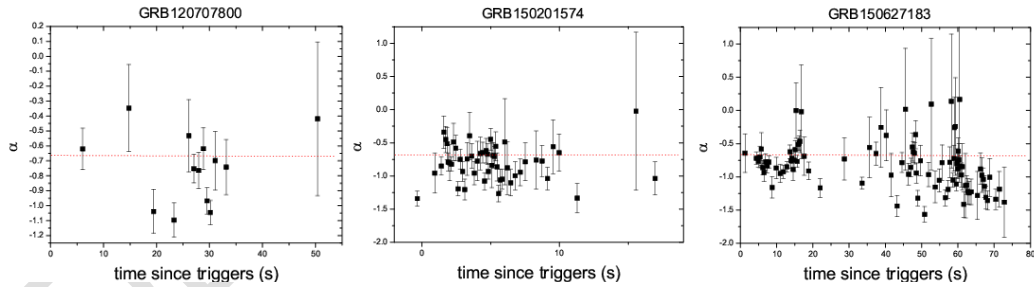


**Fig. 7** Fitting result of low-energy power law index  $\alpha$  more than  $-2/3$  scale diagram, the red line is  $\alpha=-2/3$ , Left panel : GRB 120707A ; middle panel : GRB150201A ; down panel : GRB150627A.

### CPL+BB+PL model

The new model CPL+BB+PL has been showed in Guiriec et al. (2015a), and the parameters of which can be compared with Band+BB model. Only for GRB120129A, GRB121225B, GRB130504C, GRB140206A, GRB140329A, GRB150201A, GRB150627A, GRB151227B, GRB151231A, GRB160422A, the CPL+BB+PL model can get the fitting results, but some

components have large errors. We also notice that the model could not fit most time-resolved spectra for these GRBs. For example, the model cannot fit the time-integrated spectra of GRB120707A, but a better fitting result is obtained in the time-resolved spectra. If the model is artificially constructed, why does it only appear in the time-resolved spectrum? Burgess et al. (2014a) pointed out that the time-integrated spectrum tends to cover up some important information in the energy spectrum. Therefore, it is recommended to use the time-resolved spectrum in the energy spectrum analysis.

In the time-resolved spectrum analysis, only the four bursts of GRB120707A, GRB121225B, GRB140329A, GRB151231A can be well fitted, which are listed in Table 4. And we noticed that the CPL+BB+PL model parameters  $E_p$ ,  $kT$  and  $p$  and Band+BB model parameters,  $E_p$ , and  $kT$  are similar. Therefore, we can try to limit the value of each parameter in the CPL+BB+PL model so that it can be compared with the Band+BB model. Comparing the same parameters under the two models, the parameters  $E_p$ , and  $kT$  in the CPL+BB+PL model are slightly larger than those in the Band+BB model.

It can be seen from Table 4 that the low-energy index is not unique in the time-resolved spectrum fitting of each burst. In the time-integrated spectrum of GRB120707A, GRB121225B, and GRB140329A, it fluctuates at -1, -1.1, and -0.8 respectively, which are noted as  $CPL_{-1}$ ,  $CPL_{-1.1}$ ,  $CPL_{-0.8}$ ; the value of GRB151231A fluctuates greatly. In the low energy range, the Band spectrum has the same spectrum shape as the CPL spectrum. Under the limit of synchrotron radiation, the electron fast and slow cooling processes corresponds to -0.7 and -1.5. As discussed in Section 5.1, our limit value should be less than -0.7, and we assume  $\alpha = -0.7$  of GRB151231A, recorded as  $CPL_{-0.7}$ . The thermal energy  $kT$  fluctuates in dozens of keV; the value of the power-law spectrum index  $p$  is between -1 and -2, so we choose the power-law spectrum index  $p=-1.5$ , which is recorded as  $PL_{-1.5}$  (see Table 4). For the time-integrated spectrum fitting results, the CPL+BB+PL low-energy power-law index is less than -1, and close to -1 in a few GRBs. The thermal energy  $kT$  and the power-law index  $p$  are similar for the time-resolved spectrum.

After limiting  $\alpha$  and  $p$ , the model is recorded as  $CPL_{fix} + BB + PL_{-1.5}$ , which reduces 2 degrees of freedom, and the value of C-stat/DOF is very close to Band+BB. The fitting results are given in Table 4. But we must point out that the CPL+BB+PL model and  $CPL_{fix} + BB + PL_{-1.5}$  model can get the fitting results in some time intervals, but only the latter can be used in some intervals. It is worth noting that the PL component also appears in the energy spectrum at the beginning of the fireball explosion. The PL component can also explain why the initial low-energy power law index is often less than -1 when the CPL+BB+PL model is fitted. Only in the energy spectrum analysis can we first observe the PL component.

We try to compare Band+BB, CPL+BB+PL, and  $CPL_{fix} + BB + PL_{-1.5}$  and the changes of each parameter under these models. When the three models be used together to fit the time-resolved spectrum, the changes of various parameters,  $E_p$ , and  $kT$  seem to be insignificant, but there will be mutations in a small number of time-resolved spectra. However, we must point out that when using CPL+BB+PL to fit the time-resolved spectrum, most of the PL components in the energy spectrum have large errors. Therefore, not all time-resolved spectra can be fitted with CPL+BB+PL.

**Table 4 Time-resolved spectrum fitting results for 4 bursts can be well fitted by CPL+BB+PL model**

GRB	T-start (s)	T-end (s)	model	Band/CPL			BB	PL	$F_p$ /erg s <sup>-1</sup> cm <sup>-2</sup>	Cstat/DOF
				$E_p$ /keV	$\alpha$	$\beta$	kT/keV	$\rho$		
120707A	-0.64	12.795	Band	204.0±157.0	-0.62±0.14	-2.03±0.05			1.33e-6±2.80e-8	581/360
			Band+BB	408.2±111.0	-0.92±0.46	-2.02±0.08	19.76±5.85		1.33e-6±2.90e-8	581/358
			CPL+BB+PL	308.7±36.0	-1.23±0.20		23.56±2.19	-1.44±0.45	1.35e-6±3.50e-8	582/457
			CPL <sub>-1.0</sub> +BB+PL <sub>-1.5</sub>	80.69±11.8	-1.0		20.86±1.53	-1.5	1.32e-6±3.30e-8	584/359
	12.795	16.811	Band	238.0±59.0	-0.35±0.29	-2.06±0.05			1.88e-6±5.40e-8	478/360
			Band+BB	239.3±36.2	-1.02±0.22	-2.38±0.25	13.42±1.86		1.88e-6±5.70e-8	473/358
			CPL+BB+PL	244.0±33.3	-0.23±1.42		13.98±1.69	-1.74±0.12	1.84e-6±6.10e-8	473/357
			CPL <sub>-1.0</sub> +BB+PL <sub>-1.5</sub>	113.0±18.3	-1.0		13.71±1.04	-1.5	1.85e-6±6.10e-8	474/359
	16.811	22.086	Band	236.0±33.8	-1.04±0.15	-2.23±0.10			1.54e-6±4.70e-8	531/360
			Band+BB	204.5±31.2	-1.32±0.11	<5	13.95±2.71		1.54e-6±5.50e-8	527/358
			CPL+BB+PL	185.9±22.4	-1.26±0.13		12.95±2.94	0.85±1.59	1.48e-6±6.60e-8	521/357
			CPL <sub>-1.0</sub> +BB+PL <sub>-1.5</sub>	159.8±25.9	-1.0		10.28±1.13	-1.5	1.49e-6±4.70e-8	528/359
	22.086	25.540	Band	136.6±94.2	-1.10±0.12	-2.33±0.17			2.37e-6±7.50e-8	424/360
			Band+BB	181.8±17.1	-1.09±0.19	-2.25±0.38	57.5±37.0		2.35e-6±8.40e-8	425/358
			CPL+BB+PL	194.9±23.5	-0.29±1.01		9.27±1.63	-1.62±0.23	2.26e-6±7.70e-8	418/357
			CPL <sub>-1.0</sub> +BB+PL <sub>-1.5</sub>	100.8±16.5	-1.0		9.79±1.86	-1.5	2.29e-6±7.50e-8	420/359
	25.540	26.672	Band	389.3±60.7	-0.53±0.24	-2.03±0.06			2.82e-6±8.00e-8	385/360
			Band+BB	347.2±58.7	-1.18±0.11	<-5	15.99±1.82		2.94e-6±9.40e-8	379/358
			CPL+BB+PL	318.6±42.3	-1.15±0.12		15.75±1.90	0.11±1.85	2.78e-6±1.10e-7	372/357
			CPL <sub>-1.0</sub> +BB+PL <sub>-1.5</sub>	230.7±22.9	-1.0		14.70±1.14	-1.5	2.87e-6±9.40e-8	377/359
	26.672	27.441	Band	385.1±40.3	-0.75±0.10	-2.43±0.15			6.78e-6±1.80e-7	381/360
			Band+BB	360.1±45.0	-0.93±0.10	<-5	21.69±3.43		6.99e-6±2.00e-7	372/358
			CPL+BB+PL	399.0±38.7	-0.91±0.11		21.50±3.60	1.07±2.54	6.85e-6±2.40e-7	369/357
			CPL <sub>-1.0</sub> +BB+PL <sub>-1.5</sub>	171.0±20.6	-1.0		24.06±2.77	-1.5	6.99e-6±2.50e-7	368/359
	27.441	28.453	Band	278.5±31.4	-0.76±0.12	-2.34±0.13			5.03e-6±1.40e-7	398/360
			Band+BB	285.7±26.5	-0.82±0.19	-3.29±0.92	14.41±2.18		5.04e-6±1.50e-7	389/358
			CPL+BB+PL	297.6±31.7	-0.87±0.15		15.29±2.23	-0.66±1.19	5.02e-6±1.60e-7	386/357
			CPL <sub>-1.0</sub> +BB+PL <sub>-1.5</sub>	157.1±18.5	-1.0		18.59±2.08	-1.5	5.09e-6±1.50e-7	389/359
	28.453	29.235	Band	160.5±25.1	-0.62±0.14	-2.33±0.17			5.68e-6±1.60e-7	367/360
			Band+BB	190.6±20.3	-0.31±0.68	-2.36±0.13	8.35±2.43		5.65e-6±1.60e-7	365/358
			CPL+BB+PL	230.3±25.8	-0.55±0.48		15.98±7.60	-1.503±0.23	5.42e-6±1.70e-7	358/357
			CPL <sub>-1.0</sub> +BB+PL <sub>-1.5</sub>	224.9±23.5	-1.0		29.04±4.46	-1.5	5.55e-6±1.70e-7	362/359
	29.235	29.812	Band	249.0±31.1	-0.97±0.09	-2.56±0.21			7.70e-6±2.10e-7	419/360
			Band+BB	240.0±31.1	-0.97±0.09	-2.56±0.21	11.68±1.58		7.67e-6±2.10e-7	411/358
			CPL+BB+PL	280.0±28.3	-0.61±0.33	-2.63±0.24	13.21±1.80	-1.46±0.73	7.65e-6±2.30e-7	410/357
			CPL <sub>-1.0</sub> +BB+PL <sub>-1.5</sub>	296.7±30.0	-0.78±0.35		16.03±2.36	-1.5	7.73e-6±2.30e-7	412/359
	29.812	30.511	Band	249.5±28.4	-1.0				6.70e-6±1.90e-7	452/360
			Band+BB	270.9±36.8	-1.04±0.08	-2.56±0.24	11.70±1.74		6.68e-6±1.90e-7	445/358
			CPL+BB+PL	289.9±30.9	-0.75±0.28	-2.62±0.27	12.99±2.16	0.84±1.22	6.50e-6±2.50e-7	434/357
			CPL <sub>-1.0</sub> +BB+PL <sub>-1.5</sub>	309.2±33.3	-0.90±0.17		15.04±2.23	-1.5	6.73e-6±2.00e-7	444/359
	30.511	31.616	Band	115.8±18.6	-1.0				4.25e-6±1.20e-7	399/360
			Band+BB	217.5±40.5	-0.70±0.20	-2.12±0.09	12.87±2.69		4.26e-6±1.30e-7	394/358
			CPL+BB+PL	265.0±40.5	-0.90±0.25	-2.37±0.20	14.53±2.23	-1.12±0.57	4.22e-6±1.40e-7	390/357
			CPL <sub>-1.0</sub> +BB+PL <sub>-1.5</sub>	249.6±32.0	-1.06±0.15		14.56±1.55	-1.5	4.22e-6±1.40e-7	390/359
	31.616	34.655	Band	106.2±15.0	-1.0				2.09e-6±6.50e-8	482/360
			Band+BB	126.6±27.5	-0.74±0.18		8.51±1.91		2.07e-6±6.60e-8	479/358
			CPL+BB+PL	170.8±21.8	-0.34±0.78		11.58±2.00	-1.52±0.30	2.00e-6±7.00e-8	477/359
			CPL <sub>-1.0</sub> +BB+PL <sub>-1.5</sub>	179.2±23.6	-0.76±0.50		13.76±1.77	-1.5	2.02e-6±6.40e-8	478/359
34.655	66.112	Band	43.1±7.5	-1.00				4.74e-7±1.60e-8	846/360	
		Band+BB	33.9±9.6	-0.42±0.51	-2.07±0.05	23.76±6.72		4.72e-7±1.70e-8	841/358	
		CPL+BB+PL	105.5±17.4	-0.21±0.94	-2.04±0.07	6.93±0.81	-1.5	4.52e-7±1.50e-8	827/359	
		CPL <sub>-1.0</sub> +BB+PL <sub>-1.5</sub>	381.2±48.1	-1.00				6.34e-7±1.90e-8	500/504	
-1.984	17.482	Band	572.1±185.0	-0.96±0.05	-2.19±0.21			6.50e-7±2.70e-8	498/502	
		Band+BB	591.9±197.0	-1.09±0.09	-2.36±0.40	33.13±7.06		6.57e-7±2.20e-8	499/501	
		CPL+BB+PL	646.3±86.6	-1.08±0.32		33.12±8.49	-1.45±1.04	6.57e-7±2.20e-8	499/501	
		CPL <sub>-1.1</sub> +BB+PL <sub>-1.5</sub>	502.3±75.3	-1.1		33.89±4.98	-1.5	6.59e-7±2.20e-8	499/503	
17.482	18.126	Band	3078.0±681.0	-0.68±0.07	-1.81±0.07			5.43e-6±1.70e-7	580/504	
		Band+BB	791.6±116.0	-1.06±0.04	-2.67±0.57	50.89±4.99		5.38e-6±1.70e-7	572/502	
		CPL+BB+PL	860.7±193.0	-0.94±0.04	-2.56±0.40			5.17e-6±1.70e-7	546/504	
		CPL <sub>-1.1</sub> +BB+PL <sub>-1.5</sub>	1335.0±196.0	-0.96±0.07	-2.64±0.49	31.61±33.9		5.16e-6±1.70e-7	545/502	
18.126	18.776	Band	682.8±107.0	-1.1				5.03e-6±1.50e-7	550/503	
		Band+BB	1532.0±325.0	-0.99±0.04	-2.31±0.26	61.6±12.2	-1.5	5.61e-6±2.10e-7	561/504	
		CPL+BB+PL	1454.0±220.0	-1.17±0.04	<-5	32.98±5.35		5.56e-6±1.90e-7	552/502	
		CPL <sub>-1.1</sub> +BB+PL <sub>-1.5</sub>	473.7±62.8	-1.1		32.39±4.74	-1.5	5.57e-6±1.70e-7	552/503	
18.776	19.312	Band	670.8±210.0	-0.85±0.05	-2.22±0.19			4.74e-6±1.70e-7	528/504	
		Band+BB	1093.0±174.0	-0.97±0.10	-2.32±0.28	39.43±10.50		4.79e-6±1.80e-7	526/502	
		CPL+BB+PL	548.9±75.7	-1.1		45.34±5.17	-1.5	4.74e-6±1.50e-7	532/503	
		CPL <sub>-1.1</sub> +BB+PL <sub>-1.5</sub>	1071.0±227.0	-0.26±0.05	-2.36±0.28			5.48e-6±2.10e-7	584/504	
19.312	19.970	Band	1163.0±168.0	-1.07±0.05	<-5	32.43±6.10		561e-6±1.80e-7	579/502	
		Band+BB	257.3±38.1	-1.1		33.79±5.28	-1.5	5.71e-6±1.70e-7	581/503	
		CPL+BB+PL	998.8±346.0	-0.94±0.08	-1.91±0.09			3.48e-6±1.10e-7	572/504	
		CPL <sub>-1.1</sub> +BB+PL <sub>-1.5</sub>	1103.0±399.0	-1.11±0.07	-2.55±0.61	28.22±3.31		3.76e-6±1.30e-7	561/502	
20.516	21.296	Band	1093.0±211.0	-1.1±0.35		28.63±3.32	-1.51±1.08	3.76e-6±1.40e-7	561/501	
		Band+BB	428.9±59.5	-1.1		28.56±2.63	-1.5	3.77e-6±1.30e-7	561/503	
		CPL+BB+PL	549.8±136.0	-0.88±0.05	-2.90±0.91			3.76e-6±1.60e-7	583/504	
		CPL <sub>-1.1</sub> +BB+PL <sub>-1.5</sub>	768.1±111.0	-0.97±0.10	-3.08±1.54	33.38±9.40		3.81e-6±1.60e-7	580/502	
21.296	22.062	Band	406.7±47.7	-1.1				3.91e-6±3.30e-7	585/503	
		Band+BB	409.5±72.0	-0.78±0.06	-2.40±0.27	37.86±5.33	-1.5	5.44e-6±1.90e-7	564/504	
		CPL+BB+PL	740.0±122.0	-0.78±0.10	-2.41±0.29	17.77±111.0		5.44e-6±2.10e-7	564/502	
		CPL <sub>-1.1</sub> +BB+PL <sub>-1.5</sub>	388.9±42.1	-1.1		57.16±5.90	-1.5	5.40e-6±1.90e-7	570/503	
22.062	22.551	Band	369.2±48.0	-0.75±0.06	-2.49±0.31			5.02e-6±1.80e-7	629/504	
		Band+BB	633.9±108.0	-0.68±0.12	-2.48±0.30	3.86±2.63		5.00e-6±1.80e-7	628/502	
		CPL+BB+PL	215.5±41.2	-1.1		61.4±5.76	-1.5	4.95e-6±1.80e-7	632/503	
		CPL <sub>-1.1</sub> +BB+PL <sub>-1.5</sub>								
22.551	23.117	Band	311.3±182.0	-1.06±0.08	-2.00±0.14			1.15e-6±4.40e-8	554/504	
		Band+BB	492.0±287.0	-1.19±0.18	-2.05±0.22	22.43±8.32		1.16e-6±4.40e-8	553/502	
		CPL+BB+PL	296.8±40.3	-1.29±0.45		23.90±4.98	-1.49±1.76	1.20e-6±6.20e-8	554/501	
		CPL <sub>-1.1</sub> +BB+PL <sub>-1.5</sub>	222.6±20.2	-1.1		19.66±5.03	-1.5	1.14e-6±5.20e-8	555/503	
23.117	26.126	Band	427.2±118.0	-0.92±0.05	-2.42±0.29			4.85e-7±1.70e-8	707/504	
		Band+BB	394.4±104.0	-1.27±0.09	<-5	33.10±2.76		4.98e-7±2.00e-8	704/502	
		CPL+BB+PL	285.8±29.7	-1.25±0.09		33.66±2.91	-0.06±3.74	4.92e-7±2.10e-8	703/501	
		CPL <sub>-1.1</sub> +BB+PL <sub>-1.5</sub>	210.2±36.1	-1.1		33.82±4.66	-1.5	4.79e-7±1.80e-8	705/503	
26.126	51.129	Band	109.6±222.0	-1.09±0.07	-2.23±0.27			1.16e-6±5.50e-8	579/504	
		Band+BB	95.8±514.0	-1.45±0.32	-1.75±0.11	38.05±3.63		1.11e-6±4.80e-8	563/502	
		CPL+BB+PL	45.54±21.4	-0.74±6.94		40.66±16.7	-1.70±0.18	1.09e-6±5.70e-8	563/501	
		CPL <sub>-1.1</sub> +BB+PL <sub>-1.5</sub>	206.9±15.4	-1.1		41.81±4.46	-1.5	1.06e-6±4.70e-8	564/503	
51.129	53.507	Band	252.1±55.8	-0.83±0.06	<-5			1.64e-6±7.20e-8	557/504	
		Band+BB	287.2±30.2	-1.01±0.16	<-5	28.70±5.77		1.69e-6±1.00e-7	555/502	
		CPL+BB+PL	316.7±66.7	-0.85±0.06	-2.74±0.56			4.09e-6±1.50e-7	529/504	
		CPL <sub>-1.1</sub> +BB+PL <sub>-1.5</sub>								

GRB	T-start (s)	T-end (s)	model	Band/CPL			BB	PL	F <sub>p</sub> /erg s <sup>-1</sup> cm <sup>-2</sup>	Cstat/DOF	
				E <sub>p</sub> /keV	α	β	kT/keV	ρ			
140329A	56.387	58.909	Band	173.0±44.3	-0.96±0.07	-2.99±0.99			9.77e-7±6.50e-8	596/504	
			Band+BB	85.3±8.1	-1.00±0.21	-2.88±1.03	31.08±28.50		9.79e-7±6.40e-8	586/502	
	58.909	61.306	Band	34.6±21.4	-1.17±0.09	-3.02±0.75			6.68e-7±5.10e-8	572/504	
			Band+BB	87.1±11.0	-1.32±0.46	-2.10±0.17	22.24±2.55		7.06e-7±4.60e-8	567/502	
	61.306	63.249	Band	59.84±5.62	-1.38±0.09	-2.79±0.67			7.97e-7±6.10e-8	501/504	
			CPL <sub>-1.1</sub> +BB+PL <sub>-1.5</sub>	79.8±9.9	-1.1		9.65±1.21	-1.5	7.82e-7±4.80e-8	500/503	
	63.249	66.301	Band	76.9±8.7	-1.45±0.09	-2.79±0.68			6.04e-7±4.70e-8	514/504	
			CPL <sub>-1.1</sub> +BB+PL <sub>-1.5</sub>	26.6±2.8	-1.1		18.25±2.71	-1.5	5.60e-7±3.80e-8	514/503	
	66.301	85.312	CPL <sub>-1.1</sub> +BB+PL <sub>-1.5</sub>	507.5±38.3	-1.1		7.64±0.79	-1.5	1.57e-7±1.20e-8	534/503	
			Band	143.1±16.6	-0.38±0.15	-2.17±0.12			1.28e-6±5.40e-8	382/360	
			Band+BB	327.8±127.0	-0.95±0.20	-2.53±0.68	23.9±3.19		1.29e-6±6.20e-8	382/358	
			CPL+BB+PL	373.4±123.0	-0.99±0.49		24.25±3.07	-1.45	1.31e-6±3.90e-8	382/357	
			CPL <sub>-0.8</sub> +BB+PL <sub>-1.5</sub>	298.2±38.7	-0.8		22.45±2.29	-1.5	1.28e-6±6.10e-8	384/359	
			Band	264.3±52.1	-0.80±0.12	-2.11±0.22			3.24e-7±1.60e-8	535/360	
		0.842	20.686	Band	314.5±81.0	-0.45±0.40	-2.21±0.31	13.19±1.97		3.32e-7±1.70e-8	326/358
			Band+BB	414.5±102.0	-0.71±0.72		15.20±2.66	-1.44	3.40e-7±2.20e-8	529/357	
			CPL+BB+PL	225.6±23.3	-0.81±0.08	-2.68±0.36			5.13e-6±2.00e-7	377/360	
		20.686	21.054	Band	239.2±30.3	-0.66±0.19	-2.76±0.42	10.75±2.62		5.14e-6±2.00e-7	373/358
			Band+BB	243.5±22.6	-0.32±0.67		11.97±2.44	-1.67±0.19	5.01e-6±2.10e-7	374/357	
			CPL+BB+PL	264.8±23.4	-0.8		13.01±2.44	-1.5	5.12e-6±2.10e-7	375/359	
			CPL <sub>-0.8</sub> +BB+PL <sub>-1.5</sub>	217.9±22.7	-0.61±0.09	-2.31±0.15			9.370e-6±3.20e-7	358/360	
		21.054	21.256	Band	343.8±58.9	-0.70±0.14	-2.67±0.40	18.15±2.62		7	346/358
			Band+BB	379.8±50.6	-0.74±0.36		19.16±2.32	-1.44±1.81	9.91e-6±3.60e-7	349/357	
			CPL+BB+PL	402.3±39.2	-0.8		20.13±1.81	-1.5	1.00e-5±3.80e-7	349/359	
			CPL <sub>-0.8</sub> +BB+PL <sub>-1.5</sub>	191.3±22.0	-0.62±0.10	-2.26±0.13			1.00e-5±3.70e-7	367/360	
		21.256	21.435	Band	276.7±47.7	-0.67±0.16	-2.51±0.27	15.17±2.99		9.94e-6±3.30e-7	360/358
			Band+BB	380.5±53.0	-0.88±0.40		19.54±2.70	-1.66	1.10e-5±3.60e-7	365/357	
			CPL+BB+PL	350.5±33.0	-0.8		17.91±1.82	-1.5	1.04e-5±4.00e-7	365/359	
			CPL <sub>-0.8</sub> +BB+PL <sub>-1.5</sub>	163.8±17.6	-0.43±0.12	-2.23±0.11			1.03e-5±3.90e-7	380/360	
		21.435	21.648	Band	310.2±61.3	-0.76±0.15	-2.73±0.46	19.89±3.19		8.53e-6±2.80e-7	373/358
			Band+BB	368.3±56.8	-0.88±0.34		21.42±2.66	-1.46	8.71e-6±3.20e-7	376/357	
			CPL+BB+PL	351.6±33.4	-0.8		20.53±1.82	-1.5	8.88e-6±3.50e-7	376/359	
			CPL <sub>-0.8</sub> +BB+PL <sub>-1.5</sub>	219.3±22.6	-0.71±0.08	-2.51±0.22			8.85e-6±3.40e-7	389/360	
		21.648	21.819	Band	208.2±27.3	-0.21±0.43	-2.64±0.19	9.23±1.19		1.00e-5±3.50e-7	383/358
			Band+BB	309.2±45.0	-0.88±0.15		22.12±6.76	-1.30	1.00e-5±3.50e-7	389/357	
			CPL+BB+PL	307.5±25.5	-0.8		15.39±2.67	-1.5	1.02e-5±4.00e-7	388/359	
			CPL <sub>-0.8</sub> +BB+PL <sub>-1.5</sub>	271.6±31.9	-0.86±0.07	-2.44±0.22			1.03e-5±4.00e-7	411/360	
		21.819	21.997	Band	253.1±35.1	-0.26±0.40	-2.42±0.19	9.52±0.86		1.06e-5±3.60e-7	397/358
			Band+BB	365.7±36.9	-0.77±0.36		11.45±2.01	-1.543	1.06e-5±3.60e-7	405/357	
			CPL+BB+PL	292.5±23.6	-0.8		15.82	-1.5	1.11e-5±4.20e-7	421/359	
			CPL <sub>-0.8</sub> +BB+PL <sub>-1.5</sub>	244.1±25.1	0.76±0.07	-2.89±0.43			1.07e-5±3.90e-7	353/360	
		21.997	22.147	Band	314.3±57.6	-0.89±0.13	-3.23±1.06	24.37±5.42		1.13e-5±4.40e-7	348/358
			Band+BB	325.4±54.4	-0.91±0.20		24.55±5.20	-1.41	1.14e-5±4.40e-7	349/357	
			CPL+BB+PL	294.6±24.3	-0.8		21.61±3.76	-1.5	1.15e-5±4.50e-7	350/359	
			CPL <sub>-0.8</sub> +BB+PL <sub>-1.5</sub>	199.3±22.3	-0.79±0.09	-2.45±0.21			1.14e-5±4.30e-7	347/360	
		22.147	22.343	Band	197.2±26.9	-0.65±0.25	-2.45±0.20	7.90±3.22	-1.57±1.16	8.39e-6±3.00e-7	346/358
			Band+BB	288.0±57.0	-0.99±0.41		26.04±7.30	-1.5	8.39e-6±3.10e-7	351/357	
			CPL+BB+PL	236.7±21.2	-0.8		16.52±5.22		8.42e-6±3.60e-7	352/359	
			CPL <sub>-0.8</sub> +BB+PL <sub>-1.5</sub>	125.6±14.4	-0.39±0.15	-2.16±0.09			8.21e-6±3.20e-7	379/360	
		22.343	22.595	Band	325.0±45.0	-0.90±0.11	< -5	17.78±2.01		6.52e-6±2.30e-7	369/360
			Band+BB	321.5±48.2	-0.89±0.51		17.7±2.08	-1.60	6.75e-6±2.90e-7	369/357	
			CPL+BB+PL	304.8±30.7	-0.8		16.57±1.33	-1.51	6.73e-6±3.10e-7	370/359	
		CPL <sub>-0.8</sub> +BB+PL <sub>-1.5</sub>	239.0±58.3	-0.86±0.08	-2.29±0.17			6.69e-6±2.70e-7	396/360		
	22.595	22.833	Band	279.2±30.0	-0.83±0.15	-2.32±0.21	13.94±4.17		7.68e-6±2.70e-7	392/358	
		Band+BB	328.3±45.6	-0.82±0.57		15.91±3.17	-1.59±0.58	7.68e-6±2.80e-7	401/357		
		CPL+BB+PL	313.8±31.8	-0.8		14.87±2.23	-1.5	7.70e-6±3.20e-7	402/359		
		CPL <sub>-0.8</sub> +BB+PL <sub>-1.5</sub>	286.2±30.0	-0.72±0.07	-2.47±0.22			7.65e-6±3.10e-7	366/360		
	22.833	23.014	Band	391.2±60.4	-0.86±0.10	-3.22±0.99	26.93±9.30		1.13e-5±3.80e-7	366/358	
		Band+BB	409.3±56.9	-0.89±0.09		29.24±8.52	-0.82	1.16e-5±4.40e-7	365/357		
		CPL+BB+PL	261.7±26.9	-0.86±0.07	-2.65±0.32			1.17e-5±4.20e-7	430/360		
	23.014	23.214	Band	370.4±54.1	-0.96±0.09	-3.75±2.69	19.85±3.57		9.42e-6±3.30e-7	421/358	
		Band+BB	370.5±53.1	-0.95±0.35		20.04±3.84	-1.74	9.67e-6±3.90e-7	421/357		
		CPL+BB+PL	329.9±28.2	-0.8		15.70±1.98	-1.5	9.68e-6±3.60e-7	427/359		
		CPL <sub>-0.8</sub> +BB+PL <sub>-1.5</sub>	246.1±28.5	-0.82±0.08	-2.35±0.17			9.60e-6±3.60e-7	384/360		
	23.214	23.423	Band	262.1±28.5	-0.59±0.22	-2.41±0.20	10.62±1.82		9.21e-6±3.10e-7	378/358	
		Band+BB	306.1±36.5	-0.72±0.33		12.26±2.19	-1.40±0.66	9.25e-6±3.20e-7	391/357		
		CPL+BB+PL	324.3±29.1	-0.8		13.85±2.43	-1.5	9.25e-6±3.60e-7	382/359		
		CPL <sub>-0.8</sub> +BB+PL <sub>-1.5</sub>	313.3±26.7	-0.72±0.06	-2.90±0.42			9.34e-6±3.60e-7	400/360		
	23.423	23.592	Band	329.8±34.2	-0.51±0.18	-2.98±0.47	13.05±2.22		1.27e-5±4.30e-7	393/358	
		Band+BB	347.9±32.6	-0.50±0.19		14.24±2.47	-1.33±1.16	1.27e-5±4.30e-7	393/358		
		CPL+BB+PL	510.3±40.9	-0.75±0.05	-3.24±0.62			1.28e-5±4.70e-7	416/360		
	23.592	23.705	Band	510.3±56.0	-0.75±0.07	-3.28±0.67	25.04		2.39e-5±7.70e-7	416/358	
		Band+BB	450.7±48.3	-0.73±0.06	-2.33±0.14			2.39e-5±8.00e-7	361/360		
	23.705	23.805	Band	470.0±66.8	-0.69±0.11	-2.36±0.15	16.57±8.78		2.53e-5±8.20e-7	360/358	
		Band+BB	409.9±39.5	-0.60±0.11	-2.28±0.12			2.54e-5±8.40e-7	345/360		
	23.805	23.889	Band	562.4±100.0	-0.70±0.10	-2.42±0.17	31.00±7.41		2.84e-5±8.60e-7	340/358	
		Band+BB	310.1±30.8	-0.60±0.07	-2.26±0.12			2.88e-5±9.20e-7	343/360		
	23.889	24.001	Band	523.5±88.4	-0.77±0.10	-2.58±0.26	25.79±3.87		2.21e-5±6.70e-7	332/358	
		Band+BB	597.0±67.0	-0.8		28.27±2.79	-1.5	2.28e-5±7.70e-7	334/359		
		CPL+BB+PL	266.7±30.7	-0.60±0.09	-2.11±0.09			2.30e-5±7.20e-7	382/360		
	24.001	24.106	CPL <sub>-0.8</sub> +BB+PL <sub>-1.5</sub>	306.6±48.3	-0.47±0.21	-2.18±0.11	13.45±3.09		2.07e-5±6.30e-7	377/358	
		Band	488.1±67.0	-0.76±0.23		23.47±3.66	-1.36±0.42	2.09e-5±6.60e-7	380/357		
		Band+BB	541.9±56.1	-0.8		26.47±2.93	-1.5	2.16e-5±7.30e-7	381/359		
		CPL+BB+PL	313.9±27.5	-0.55±0.07	-2.46±0.17			2.17e-5±7.10e-7	366/360		
	24.106	24.193	CPL <sub>-0.8</sub> +BB+PL <sub>-1.5</sub>	662.3±84.6	-0.89±0.07	< -5	35.06±3.92		2.72e-5±8.30e-7	358/360	
		Band	581.8±46.6	-0.8		30.96±3.10	-1.5	2.85e-5±8.90e-7	360/359		
		Band+BB	293.2±35.9	-0.78±0.07	-2.18±0.11			2.23e-5±2.23e-5	363/360		
	24.193	24.290	CPL <sub>-0.8</sub> +BB+PL <sub>-1.5</sub>	440.8±94.8	-0.91±0.10	-2.37±0.20	23.03±6.17		2.13e-5±6.60e-7	361/358	
		Band	538.7±88.5	-0.99±0.10		26.49±4.84	-1.27±0.57	2.18e-5±7.50e-7	361/357		
		Band+BB	464.8±44.9	-0.8		22.10±3.10	-1.5	2.23e-5±7.30e-7	362/359		
		CPL+BB+PL	274.3±21.2	-0.62±0.07	-2.92±0.35			2.23e-5±7.50e-7	347/360		
	24.290	24.390	Band	266.9±24.4	-0.38±0.25	-2.86±0.31	9.72±2.03		1.94e-5±6.40e-7	345/358	
		Band+BB	317.5±35.3	-0.69±0.14		25.14±10.60	-1.29±1.25	1.94e-5±6.30e-7	347/357		
		CPL+BB+PL	208.1±22.9	-0.59±0.09	-2.25±0.12			1.96e-5±6.90e-7	361/360		
	24.390	24.510									

GRB	T-start (s)	T-end (s)	model	Band/CPL			BB	PL	F <sub>p</sub> /erg s <sup>-1</sup> cm <sup>-2</sup>	Cstat/DOF
				E <sub>p</sub> /keV	α	β	kT/keV	ρ		
151231A	24.793	24.965	Band	170.7±20.4	-0.59±0.11	-2.17±0.10			1.14e-5±4.40e-7	368/360
			Band+BB	180.3±29.3	-0.24±0.44	-2.21±0.11			1.01e-5±3.40e-7	363/358
			CPL+BB+PL	276.6±36.5	-0.69±0.50		9.37±1.77	-1.48±0.44	1.02e-5±3.40e-7	371/357
	24.965	25.167	CPL+BB+PL	301.9±30.6	-0.8		17.17±3.32	-1.5	1.00e-5±4.00e-7	371/359
			CPL <sub>-0.8</sub> +BB+PL <sub>-1.5</sub>	218.6±24.4	-0.86±0.08	-2.60±0.27	19.83±2.45		1.02e-5±3.90e-7	396/360
			Band	234.4±30.0	-0.46±0.30	-2.64±0.30			8.21e-6±3.00e-7	384/358
	25.167	25.455	Band+BB	289.8±27.5	-0.81±0.15		9.93±1.10	-1.21	8.24e-6±3.00e-7	386/357
			CPL+BB+PL	293.7±25.5	-0.8		12.37±1.86	-1.5	8.35e-6±3.40e-7	385/359
			CPL <sub>-0.8</sub> +BB+PL <sub>-1.5</sub>	143.5±19.1	-0.84±0.11	-2.34±0.16	11.83±1.41		8.37e-6±3.40e-7	406/360
	25.455	25.832	Band	365.0±110.0	-1.37±0.11	< -5			5.14e-6±3.10e-7	409/358
			Band+BB	354.2±138.0	-1.37±0.12		25.83±2.83	-1.10	5.29e-6±2.30e-7	409/357
			CPL+BB+PL	152.8±103.6	-0.8		25.88±2.85	-1.5	5.27e-6±2.40e-7	415/359
	25.832	26.307	CPL <sub>-0.8</sub> +BB+PL <sub>-1.5</sub>	109.7±13.1	-0.64±0.14	-2.24±0.11	23.35		4.83e-6±1.90e-7	328/360
			Band	229.9±21.8	-0.76±0.18	< -5			4.23e-6±1.70e-7	314/358
			Band+BB	252.1±42.3	-1.00±0.56		10.66±0.99	-1.57	4.19e-6±1.90e-7	317/357
	26.949	28.153	CPL+BB+PL	230.9±22.7	-0.8		13.03±1.61	-1.5	4.31e-6±1.90e-7	314/359
			CPL <sub>-0.8</sub> +BB+PL <sub>-1.5</sub>	118.8±13.1	-0.71±0.13	-2.46±0.19	11.36±1.96		4.24e-6±1.90e-7	382/360
			Band	141.4±20.8	-0.39±0.41	-2.62±0.29			3.05e-6±1.40e-7	377/358
	28.153	35.136	Band+BB	161.1±18.1	-0.8		8.63±1.47	-1.5	3.02e-6±1.40e-7	383/359
			CPL+BB+PL	101.4±15.4	-0.80±0.16	-2.16±0.11	11.36±1.96		2.90e-6±1.37e-7	377/360
			Band	104.1±22.0	-0.01±1.17	-2.18±0.17			2.46e-6±1.10e-7	374/358
	-3.584	3.478	Band+BB	127.3±10.9	-1.10±0.08	< -5	6.28±0.85		2.45e-6±1.10e-7	427/360
			Band	203.6±71.6	-1.18±0.58				1.21e-6±5.80e-8	383/359
			CPL+BB+PL	53.65±11.5	-0.71±0.38	-2.23±0.16	11.36±1.96	-1.57±0.90	2.90e-6±1.30e-7	473/360
	3.478	5.006	Band	135.4±23.8	-1.30±0.14	-2.48±0.25			2.56e-7±2.20e-8	392/360
			Band+BB	162.1±29.5	-0.71±2.48	-2.56±0.25			1.12e-6±4.20e-8	374/358
			CPL+BB+PL	186.4±19.7	-1.32±0.35		9.38±1.07	-1.69±0.42	1.10e-6±4.00e-8	377/357
	5.006	5.884	CPL <sub>-0.7</sub> +BB+PL <sub>-1.5</sub>	192.7±21.9	-0.7		9.50±1.32	-1.5	1.07e-6±4.30e-8	378/359
			Band	217.0±17.1	-0.84±0.09	-2.79±0.27	9.35±0.75		1.07e-6±3.80e-8	434/360
			Band+BB	226.3±21.5	-0.13±0.65	-0.77±0.23			4.29e-6±1.10e-7	423/358
	5.884	6.778	CPL+BB+PL	293.2±39.8	-0.89±0.53		12.10±1.21	-1.88	4.27e-6±1.10e-7	437/357
			Band	516.6±46.0	-0.7		18.87±3.47	-1.5	4.29e-6±1.00e-6	428/359
			CPL <sub>-0.7</sub> +BB+PL <sub>-1.5</sub>	379.3±30.7	-0.84±0.07	-2.71±0.25	14.83±1.71		4.30e-6±1.40e-7	354/360
	6.778	7.840	Band	500.1±51.0	-0.78±0.12	-3.20±0.64			8.78e-6±2.10e-7	338/358
			Band+BB	419.9±26.1	-0.7		24.83±3.32	-1.5	8.90e-6±2.20e-7	339/358
			CPL <sub>-0.7</sub> +BB+PL <sub>-1.5</sub>	381.8±31.3	-0.85±0.07	-2.69±0.25	25.40±3.21		8.95e-6±2.00e-7	415/360
	7.840	12.128	Band	501.3±57.8	-0.83±0.11	-3.05±0.54			8.02e-6±1.90e-7	400/358
			Band+BB	417.6±28.3	-0.7		27.22±4.18	-1.5	8.10e-6±2.00e-7	406/359
			CPL <sub>-0.7</sub> +BB+PL <sub>-1.5</sub>	333.3±30.7	-0.98±0.07	-2.73±0.31	27.54±3.92		8.24e-6±1.90e-7	376/360
	12.128	64.167	Band	366.3±39.5	-0.86±0.16	-2.87±0.41			6.43e-6±1.60e-7	372/358
			Band+BB	442.5±53.2	-1.08±0.08		15.85±3.69	-0.16±5.55	6.44e-6±1.70e-7	378/359
			CPL+BB+PL	370.7±26.5	-0.7		29.83±7.07	-1.5	6.54e-6±1.70e-7	376/359
	64.167	65.754	CPL <sub>-0.7</sub> +BB+PL <sub>-1.5</sub>	200.1±21.8	-0.71±0.13	-2.34±0.13	15.05±1.84		6.47e-6±1.60e-7	473/360
			Band	273.4±79.6	-0.89±0.24	-2.51±0.17			2.15e-6±5.70e-8	471/358
			Band+BB	364.4±43.3	-0.84±0.31		24.64±8.26	-1.43±0.39	2.15e-6±5.90e-8	467/359
	65.754	67.928	CPL+BB+PL	253.1±28.2	-0.7		24.53±6.96	-1.5	2.11e-6±6.70e-8	467/359
			CPL <sub>-0.7</sub> +BB+PL <sub>-1.5</sub>	179.7±27.4	-1.15±0.14	-2.84±0.68	22.64±4.02		2.10e-6±5.80e-8	458/360
			Band	78.0±79.1	-1.38±0.61	-2.11±0.28			3.01e-7±1.50e-8	455/358
	67.928	69.925	Band+BB	56.63±72.9	-0.81±2.71		47.27±7.76	-1.94±0.11	2.99e-7±1.40e-8	454/357
			CPL+BB+PL	167.1±18.5	-0.7		50.76±17.4	-1.5	2.93e-7±1.60e-8	456/359
			CPL <sub>-0.7</sub> +BB+PL <sub>-1.5</sub>	219.7±20.8	-0.84±0.10	-2.53±0.18	6.19±2.04		2.90e-7±1.20e-8	360/361
	69.925	71.452	Band	314.8±65.1	-1.08±0.15	-2.91±0.63			4.21e-6±1.10e-7	358/358
			Band+BB	302.9±46.0	-1.08±0.13		30.04±6.94	0.50±1.96	4.24e-6±1.20e-7	353/357
			CPL+BB+PL	246.7±23.2	-1.5		30.81±6.81	-1.5	4.16e-6±1.50e-7	361/359
	71.452	90.624	CPL <sub>-0.7</sub> +BB+PL <sub>-1.5</sub>	219.8±15.9	-0.90±0.09	-3.30±0.70	19.75±4.10		4.11e-6±1.10e-7	403/360
			Band	223.9±17.3	-0.54±0.37	-3.21±0.52			3.05e-6±8.90e-8	400/358
			Band+BB	223.1±16.8	-0.89±0.09		10.30±1.77	-1.34±0.63	3.03e-6±9.00e-8	399/357
	90.624	90.624	CPL+BB+PL	222.5±16.4	-0.7		10.42±1.85	-1.5	2.98e-6±9.20e-8	399/359
			CPL <sub>-0.7</sub> +BB+PL <sub>-1.5</sub>	134.6±10.7	-0.34±0.17	-2.75±0.18	10.59±2.98		3.01e-6±8.50e-8	426/360
			Band	167.6±58.0	-0.64±0.55	-2.87±0.33			2.87e-6±8.70e-8	426/358
90.624	90.624	Band+BB	144.8±7.45	-0.55±0.79		23.30±8.75	-1.65±0.50	2.86e-6±9.00e-8	426/357	
		CPL+BB+PL	180.3±18.3	-0.7		22.41±7.21	-1.5	2.79e-6±9.10e-8	427/359	
		CPL <sub>-0.7</sub> +BB+PL <sub>-1.5</sub>	164.8±9.38	-0.59±0.11	-3.36±0.45	24.17±3.04		2.79e-6±8.10e-8	392/60	
90.624	90.624	Band	186.4±14.9	-0.11±0.56	-3.44±0.52			3.63e-6±1.10e-7	387/358	
		Band+BB	197.3±25.2	-0.05±1.06		13.44±1.96	-1.88±0.46	3.60e-6±1.10e-7	388/357	
		CPL+BB+PL	198.7±17.1	-0.7		15.08±2.71	-1.5	3.55e-6±1.00e-7	390/359	
90.624	90.624	CPL <sub>-0.7</sub> +BB+PL <sub>-1.5</sub>	81.4±11.9	-0.02±0.51	-2.34±0.12	18.69±3.02		3.63e-6±1.10e-7	394/360	
		Band	131.3±43.5	0.39±3.62	-2.47±0.25			4.58e-7±2.20e-8	392/358	
		Band+BB	142.1±47.4	0.31±3.42		11.63±2.94	-1.60±0.32	4.53e-7±2.30e-8	394/357	
90.624	90.624	CPL+BB+PL	140.3±29.8	-0.7		13.06±2.56	-1.5	4.39e-7±2.60e-8	394/359	
		CPL <sub>-0.7</sub> +BB+PL <sub>-1.5</sub>				15.23±2.36				

## DISCUSSION AND CONCLUSIONS

According to the time-integrated and time-resolved analysis results, the spectra can be modeled with a combination of non-thermal component (Band/CPL) and thermal component (BB), and the extra power law component can be modeled in the low-energy band. **Based on the standard fireball model the spectra should be thermal, but most of the observed spectra are non-thermal.** In this section, we mainly discuss the fitting results and spectral evolution of Band+BB.

### the low-energy index $\alpha$

The value of  $\alpha$  slightly softens when adding a BB to the Band for most GRBs, but the scenario does not occur for the value of  $\beta$ . In other words, the thermal component mainly affects the low-energy spectra and the effect of the high-energy range is not obvious in GRBs time-resolved spectra. In addition, the values of low-energy power-law index  $\alpha$  of empirical Band function is less than  $-2/3$  and  $-3/2$ , which correspond to the slow- and fast-cooling synchrotron radiation, respectively (Sari et al. 1998). And the radiative electron would be accelerated to relativistic velocity due to the collision in the internal shock model, so that the  $\alpha$  are not beyond  $-2/3$  because relativistic electron will fast cool after the collision (Katz 1994). In our fitting results, there are only four bursts **satisfying** with the internal-shock synchrotron radiation.

For **GRB121225B**, all the values of  $\alpha$  are less than  $-2/3$  and vary between  $-1.5$  and  $-1$  in our fitting results. It implies that **GRB121225B** agrees well with fast-cooling synchrotron radiation; For **GRB130518A**, except the time interval  $26.714 \sim 27.277$  s, the values of  $\alpha$  vary from  $-0.64$  to  $-1$ , which can be regarded as slow-cooling synchrotron radiation; For GRB151227B, except the time interval  $30.219 \sim 30.624$  s, the values of  $\alpha$  are closed to or less than  $-1$ , which is similar to GRB121225B; For GRB160422A, the variation range of  $\alpha$  is large than others, but the value is cluster in  $-1.1$  which is satisfied with fast-cooling synchrotron radiation.

**On the other hand**, the radiative efficiency of internal shock model is too less according to observation (Boucher et al. 2009). Some studies show the efficiency can increase through the continuous collision after the first accelerating (Spada et al. 2001), or if there are about  $1/2$  prompt emission radiation rooting in the thermal radiation, the low-efficiency non-thermal radiation will occur.

To deal with the problems in the internal shock model, one way is that the  $\gamma$  photons are produced by other radiative mechanisms. If the electron's transverse deflections are much less than the beaming angle in a random and small-scale magnetic fields, the radiative mechanism is not synchrotron radiation but jitter radiation (Medvedev 2000). Medvedev (2006) presented that the value of  $\alpha$  of jitter radiation ranges from  $0$  to  $-1$ , which depend on the angle of line-of-sight. This model can naturally explain the typical value,  $\alpha=-1$ , of GRB observations and predicts that about a quarter of time-resolved spectra should have hard values of  $\alpha$ , which violates the synchrotron line of death. In our fitting results, there are just three bursts agree well with the jitter radiation, we showed it in Figure 7, and the ratio beyond  $-2/3$  is 23.08%, 21.98%, 21.95% of **GRB120707A**, **GRB150627A**, **GRB150201A**, respectively. However, the small-scale magnetic field assumed in the jitter radiation actually could not be reproduce from relativistic shocks in numerical simulations (Sironi & Spitkovsky 2009), which indicates that jitter radiation is not a credible candidate of radiative mechanism in GRB prompt emission. Except for the mechanism we have mentioned above, the self-synchrotron radiation (SSC) is always used to explain the  $\gamma$  photons emission.

However, the synchrotron radiation seems remain a better model to explain a large proportion of the prompt emissions, so that sometimes we must give up the internal shock model. If the magnetic field in the Internal-collision-induced Magnetic Reconnection and Turbulence (**ICMART**) model is strong enough, the radiative electrons will be accelerated by the reconnection until it ends (Narayan & Kumar 2009), and the deadline of internal shock fast-cooling synchrotron radiation can be avoided. Besides, the simulation of **ICMART** model pointed out that there are two components in the instantaneous radiation light curve: the slow component produced by the reconnection event and the fast component produced by the shell collision, and the observations have also confirmed by the theoretical prediction (Gao & Zhang 2012).

### the $E_p - kT$ relation

The jet component of prompt emission has been discussed in several decades, and it can be divided into two classes, matter-dominant and magnetic-dominant. Burgess et al. (2014b) showed there are a linear correlation between the characteristic parameters of non-thermal and thermal component, the peak energy  $E_p$  and the thermal temperature  $kT$ ,  $E_p \propto kT^\delta$ , and the value of  $\delta$  can be interpreted by the jet dominated by magnetic or kinetic energy, which is equal to  $6(3\mu - 1)/(14\mu - 5)$  and  $1.2$ , respectively, where  $\mu$  depends on the bulk Lorentz factor and the radius,  $\Gamma \propto R^\mu$ . We showed our results in Table 5 and the eight **example** burst correlations have presented in Figure 8. The value of  $\delta$  is between  $0$  and  $0.8$ . We can get that  $\mu$  floats around  $0.31$  by  $6(3\mu - 1)/(14\mu - 5) = \delta$  and the values of  $\mu$  for each burst indicated that the jet is magnetic-dominant. Therefore, in the Band(+BB) model, the  $\delta$  of magnetic-dominant jet is about  $0.5$ . We make sure the jet component through the  $E_p - kT$  relation. Similar scenario has been found in

GRB080916C. It has been suggested that there is a magnetically dominated outflow entrained with baryonic matters, which indicates that the thermal component is weak in a Poynting flux (Zhang & Pe'er 2009).

We noticed that in some bursts such as GRB120707A, the fitting results of the Band+BB model was weak or even negative ( $r = -0.2188$ ,  $P = 0.4727$ ), while in the CPL+BB+PL model the linear correlation becomes stronger ( $r = 0.7807$ ,  $P = 0.0027$ ). Therefore, it can be approximated that there is a linear relationship, which also shows that the CPL+BB+PL model does exist in the GRB instantaneous radiation energy spectrum. Additionally, a hybrid jet is composed of thermal (hot fireball) component and non-thermal (cold Poynting flux) component if the fireball expands first thermally and then magnetically and with such a hybrid jet the mechanism is likely ICMART to power the non-thermal emission (Gao & Zhang 2015). From Table 5 there is a significant thermal component in the time-resolved spectra of the eight bursts, which implies that there are hybrid jets in most GRBs.

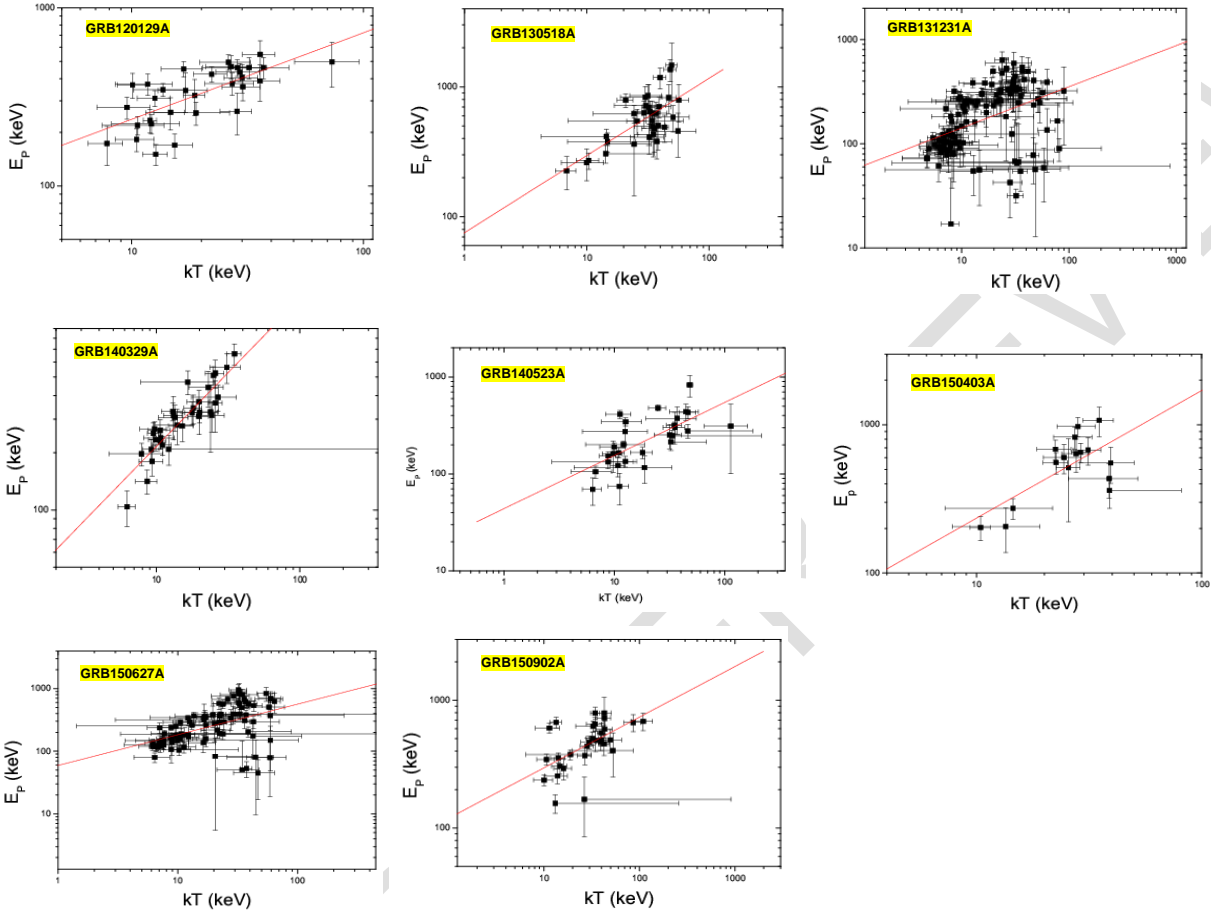


Fig. 8 A example plot of  $E_p$ - $kT$  correlation. The red line is the best fitting line of the data.

Table 5 Fitting results of  $E_p$ - $kT$  linear relationship of Band+BB model

GRB	$\delta$	$\mu$	$r$	$P$
120129580	$0.49 \pm 0.09$	$0.282 \pm 0.01$	0.7062	$< 1 \times 10^{-4}$
120707800	$0.27 \pm 0.37$	—	-0.2188	0.4727
121225417	$0.50 \pm 0.50$	—	0.2665	0.2852
130305486	$-0.18 \pm 0.17$	—	-0.4005	0.3255
130502327	$0.17 \pm 0.16$	—	0.2356	0.2791
130504978	$0.11 \pm 0.12$	—	0.1310	0.3911
130518580	$0.59 \pm 0.11$	$0.313 \pm 0.01$	0.6901	$< 1 \times 10^{-4}$
130606497	$0.23 \pm 0.11$	—	0.2332	0.0339
131231198	$0.39 \pm 0.08$	$0.323 \pm 0.01$	0.4184	$< 1 \times 10^{-4}$
140206275	$0.80 \pm 0.48$	—	0.4187	0.1203
140329295	$0.78 \pm 0.07$	$0.297 \pm 0.01$	0.8890	$< 1 \times 10^{-4}$

140523129	0.55±0.11	0.308±0.02	0.6870	< 1×10 <sup>-4</sup>
150201574	0.27±0.10	–	0.3522	0.0131
150314205	0.47±0.28	–	0.2707	0.1103
150403913	0.86±0.25	0.320±0.08	0.6743	0.0042
150627183	0.49±0.10	0.285±0.01	0.4764	< 1×10 <sup>-4</sup>
150902733	0.40±0.11	0.319±0.01	0.5715	0.0009
151227218	0.11±0.25	–	0.1049	0.6788
151231443	0.06±0.34	–	0.0519	0.8728
160422499	-0.03±0.02	–	-0.0021	0.9883

From left to right are the names of GRBs,  $\delta$ : Ep-kT linear relationship index; parameters  $\mu$ ; r: linear correlation coefficient; P: **chance probability**.

UNDER PEER REVIEW

### 5.3 The $E_p - F_p$ relation

Most studies show that there is a linear relation between the rest frame peak energy  $E_{p,z}$  and isotropic luminosity  $L_{iso}$ ,  $L_{iso} \propto E_{p,z}^k$ , where  $k$  is the power law index (Yonetoku et al. 2004, Lu et al. 2012). The parameter  $E_{p,z}$  ( $E_p(1+z)$ ) and  $L_{iso}$  ( $4\pi d_L^2 F_p$ ) can be measured by the redshift and the parameters of observations, where  $d_L$  is the luminosity distance in units of  $cm$ ;  $F_p$  is the peak flux of  $\nu F_\nu$  spectra in units of  $erg\ s^{-1}\ cm^{-2}$ ;  $z$  is the redshift.

Therefore, we present the linear relation,  $F_p \propto E_p^k$  of the 20 bursts in Table 6. The linear correlation of Band Only is better than those in Band+BB, and the value of  $k$  is between 0 to 3. Besides, the average value of  $k$  is +1.45 in Band Only which is close to the results presented by Guiriec et al. (2013), which seems to be intrinsic in the time-resolved spectra of GRB. However, fitting to the data with Band+BB does not lead to the linear correlation. Guiriec et al. (2015a) have proposed that if the additional component of the spectra is very intense, it will lead to large scatters, a weaker and biased relation or even no correlation at all. From Table 6, the significant thermal component contribution in the prompt emission spectra of the 20 bursts might bring about the weaker correlation.

**Table 6 The  $E_p$ - $F_p$  relationship in two different models**

GRB	model	k	r	P
120129A	Band	1.94±0.26	0.8092	<1×10 <sup>-4</sup>
	Band+BB	2.37±0.27	0.8502	<1×10 <sup>-4</sup>
120707A	Band	1.47±0.25	0.8746	<1×10 <sup>-4</sup>
	Band+BB	0.92±0.27	0.7138	0.0061
121225B	Band	1.06±0.20	0.7841	<1×10 <sup>-4</sup>
	Band+BB	0.54±0.17	0.6326	0.0049
130305A	Band	2.95±2.53	0.4299	0.2878
	Band+BB	None		
130502B	Band	0.84±0.25	0.436	0.0017
	Band+BB	1.45±0.60	0.3341	0.0203
130504C	Band	1.30±0.16	0.7695	<1×10 <sup>-4</sup>
	Band+BB	0.86±0.18	0.5861	<1×10 <sup>-4</sup>
130518A	Band	2.06±0.51	0.5801	0.0003
	Band+BB	1.38±0.38	0.5410	0.0009
130606B	Band	0.84±0.05	0.8695	<1×10 <sup>-4</sup>
	Band+BB	0.75±0.07	0.7777	<1×10 <sup>-4</sup>
131231A	Band	0.72±0.08	0.6290	<1×10 <sup>-4</sup>
	Band+BB	0.58±0.08	0.5459	<1×10 <sup>-4</sup>
140206A	Band	1.04±0.43	0.5714	0.0328
	Band+BB	0.59±0.25	0.5576	0.0383
140329A	Band	1.89±0.31	0.7247	<1×10 <sup>-4</sup>
	Band+BB	1.09±0.38	0.4593	0.0072
140523A	Band	1.11±0.18	0.7531	<1×10 <sup>-4</sup>
	Band+BB	0.97±0.25	0.6044	0.0007
150201A	Band	1.91±0.18	0.8189	<1×10 <sup>-4</sup>
	Band+BB	1.23±0.24	0.8057	<1×10 <sup>-4</sup>
150314A	Band	1.44±0.23	0.7940	<1×10 <sup>-4</sup>
	Band+BB	0.29±0.19	0.2110	0.1257
150403A	Band	1.47±0.28	0.7940	<1×10 <sup>-4</sup>
	Band+BB	0.47±0.39	0.3079	0.2461
150627A	Band	1.00±0.11	0.6773	<1×10 <sup>-4</sup>
	Band+BB	0.72±0.11	0.5707	<1×10 <sup>-4</sup>
150902A	Band	1.48±0.26	0.7314	<1×10 <sup>-4</sup>
	Band+BB	1.44±0.39	0.5743	0.0009
151227B	Band	1.44±0.24	0.8275	<1×10 <sup>-4</sup>
	Band+BB	0.86±0.38	0.4923	0.0380
151231A	Band	2.22±0.52	0.8043	0.0016
	Band+BB	1.78±0.26	0.9071	<1×10 <sup>-4</sup>
160422A	Band	1.40±0.10	0.8868	<1×10 <sup>-4</sup>
	Band+BB	1.29±0.10	0.8811	<1×10 <sup>-4</sup>

Among the 20 selected bursts, we only know the redshift of GRB150403A. The isotropic luminosity  $L_{iso}$  and the peak energy  $E_{p,z}$  in the rest frame obtained by two different models can be calculated by the redshift. The correlations between  $L_{iso}$  and  $E_{p,z}$  are showed in Figure 9. The results showed that the BB component indeed change the correlation of the isotropic luminosity  $L_{iso}$  and the peak energy  $E_{p,z}$ . In the early research work, Liang et al. (2004) obtained the similar results to Yonetoku with 2048 GRB time-resolved spectra observed by BATSE. After defining a parameter  $\omega$  related to the redshift and limiting the parameters of the fireball without correlation, the internal shock and the external shock model in the fireball can better explain this linear relationship and the values of the parameter  $\omega$ . However, it requires a higher requirement for the fireball. Some studies indicated that if the prompt radiation process of the GRBs satisfies the synchrotron radiation mechanism, then there is a linear relationship similar to blazars between the synchrotron luminosity  $L_{syn}$  and the Doppler factor  $D$ ,  $L_{syn} \propto D^{3.1}$ . When the Doppler factor and redshift were corrected, there is a similar  $E_{p,z}$ - $L_{iso}$  relationship between them. It shows that the jets between the GRBs and the blazars are very likely to come from the same radiation process. At the radiation spectrum of 5GHz, there is a similar linear relationship between luminosity  $L_\nu$  and  $\nu_{peak}$ , in GRBs and active galactic nucleus. That is, the radiation process of GRB and active galactic nucleus satisfies the synchronous accelerated radiation (Wu et al. 2011).

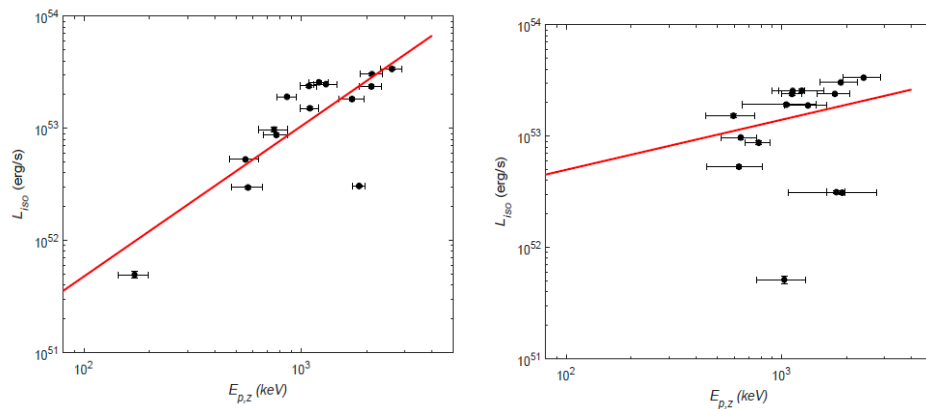


**Fig. 9** The correlations between the isotropic luminosity  $L_{iso}$  and the peak energy  $E_{p,z}$  of GRB 150403A with band and band+BB model. Left panels: Band model, Spearman correlation coefficient  $r = 0.81$  and the chance probability  $P < 0.0001$ . Right panels: Band+BB model,  $E_{p,z}$ - $L_{iso}$  Spearman correlation coefficient  $r = 0.38$  and the chance probability  $P = 0.1607$ .

### The spectral component

Generally speaking, the spectra of GRB prompt emission can be fitted with thermal and non-thermal component. We would like to discuss the origin of each component from the sub-photosphere emission and photosphere emission. If the energy dissipates below or closed to the photosphere, the electron will be accelerated by the dissipative process, the  $\gamma$  photons will be produced by synchrotron radiation at low-energy band, i.e. keV  $\sim$  MeV band (Rees & Mészáros 2005; Chhotray & Lazzati 2015), and the Comptonized process at high-energy band. Such a mechanism will lead to a single more complex shape than Band or CPL. That is, the spectra cannot be fitted with multi-component model. On the other hand, the electron surrounding the source will be accelerated by the dissipative energy from the fireball. Subsequently, the high-energy electron distribution will be in quasi-static under the combined action of the acceleration by external shock and the IC process, and the temperature will be greater than that of the photosphere (Pe'er 2013).

If there is no energy dissipation below the photosphere or the dissipation does not significantly affected the photosphere, the special geometry of the photosphere remains thermal (Lundman et al. 2013; Pe'er 2008). In this scenario, the non-thermal component might be produced by the optically thin synchrotron radiation, the emission electrons would be accelerated by internal shock (Rees & Mészáros 1994; Sari et al. 1998) and magnetic reconnection (Zhang & Yan 2011). The extra PL component can be modeled in multi-component model in early stage of the prompt emission, which indicates the physical origin of this component is internal origin instead of the external shock, and the PL photons might be produced by the Compton scattering in Thomson regime (Guiriec et al. 2015a).

## CONSENT (WHERE EVER APPLICABLE)

All authors declare that 'written informed consent was obtained from the patient (or other approved parties) for publication of this case report and accompanying images'.

## ETHICAL APPROVAL (WHERE EVER APPLICABLE)

This study is not against the public interest, or that the release of information is allowed by legislation.

## REFERENCES

1. Band D, Matteson J, Ford L, Schaefer B, Palmer D, Teegarden B, et al. BATSE Observations of Gamma-Ray Burst Spectra. I. Spectral Diversity. *The Astrophysical Journal*, 1993, 413, 281-292, [10.1086/172995](https://doi.org/10.1086/172995).
2. Bhat P, Guiriec S. An overview of the current understanding of Gamma Ray Bursts in the Fermi era. *Bulletin of the Astronomical Society of India*, 2011; 39(3), 471-515
3. Burgess J M. On spectral evolution and temporal binning in gamma-ray bursts. *Monthly Notices of the Royal Astronomical Society*, 2014, 445(3), 2589-2598. [10.1093/mnras/stu1925](https://doi.org/10.1093/mnras/stu1925).
4. Burgess J M, Preece R D, Ryde F, Veres P, Mészáros P, Connaughton V, et al. An Observed Correlation between Thermal and Non-thermal Emission in Gamma-Ray Bursts. *The Astrophysical Journal Letters*, 2014b, 784(2), L43-L47. [10.1088/2041-8205/784/2/L43](https://doi.org/10.1088/2041-8205/784/2/L43).
5. Crider A, Liang E P, Smith I A, Preece R D, Briggs M S, Pendleton G N, et al. Evolution of the Low-Energy Photon Spectral in Gamma-Ray Bursts. *The Astrophysical Journal*, 1997, 479, L39 -L42. [10.1086/310574](https://doi.org/10.1086/310574).
6. Chhotray A, Lazzati D. Gamma-ray Burst Spectra and Spectral Correlations from Sub-photospheric Comptonization. *The Astrophysical Journal*, 2015, 802(2), 132-142. [10.1088/0004-637X/802/2/132](https://doi.org/10.1088/0004-637X/802/2/132).
7. Dai Z.G., Lu T., Gamma-Ray Bursts and Afterglows from Rotating Strange Stars and Neutron Stars, *PRL*, 1998, 81, 4301-4304. [10.1103/PhysRevLett.81.4301](https://doi.org/10.1103/PhysRevLett.81.4301).
8. Daigne F, Mochkovitch R. The Expected Thermal Precursors of Gamma-Ray Bursts in the Internal Shock Model. *AIP Conference Proceedings*, 2003, 662, 289-291. [10.1063/1.1579361](https://doi.org/10.1063/1.1579361).
9. Fryer C L, Woosley S E, Hartmann D H. Formation Rates of Black Hole Accretion Disk Gamma-Ray Bursts. *The Astrophysical Journal*, 1999, 526(1), 152-177. [10.1086/307992](https://doi.org/10.1086/307992).
10. Gao H, Zhang B.-B, Zhang B, Stepwise Filter Correlation Method and Evidence of Superposed Variability Components in Gamma-Ray Burst Prompt Emission Light Curves. *The Astrophysical Journal*, 2012, 748(2), 134-148. [10.1088/0004-637X/748/2/134](https://doi.org/10.1088/0004-637X/748/2/134).
11. Geng J, Li B, Huang, Y., Repeating fast radio bursts from collapses of the crust of a strange star, *The Innovation*, 2021, 2, 100152. [10.1016/j.xinn.2021.100152](https://doi.org/10.1016/j.xinn.2021.100152)
12. Goodman J. Are gamma-ray bursts optically thick? *Astrophysical Journal*, 1986, 308, L47-L50. [10.1086/184741](https://doi.org/10.1086/184741).
13. Guiriec S, Connaughton V, Briggs M S, Burgess M, Ryde F, Daigne F, et al. Detection of a Thermal Spectral Component in the Prompt Emission of GRB 100724B. *The Astrophysical Journal*, 2011, 727(2), L33-L37. [10.1088/2041-8205/727/2/L33](https://doi.org/10.1088/2041-8205/727/2/L33).
14. Guiriec S, Daigne F, Hascoët R, Vianello G, Ryde F, Mochkovitch R, et al. Evidence for a Photospheric Component in the Prompt Emission of the Short GRB 120323A and Its Effects on the GRB Hardness-Luminosity Relation. *The Astrophysical Journal*, 2013, 770(1), 32-57. [10.1088/0004-637X/770/1/32](https://doi.org/10.1088/0004-637X/770/1/32).
15. Guiriec S, Kouveliotou C, Daigne F, Zhang B, Hascoët R, Nemmen R S, et al. Toward a Better Understanding of the GRB Phenomenon: a New Model for GRB Prompt Emission and its Effects on the New  $L_i^{NT} - E_{peak,i}^{rest,NT}$  Relation. *The Astrophysical Journal*, 2015a, 807(2), 148-202. [10.1088/0004-637X/807/2/148](https://doi.org/10.1088/0004-637X/807/2/148).
16. Guiriec S, Mochkovitch R, Piran T, Daigne F, Kouveliotou, C.; Racusin, J., et al. GRB 131014A: A Laboratory for Studying the Thermal-like and Non-thermal Emissions in Gamma-Ray Bursts, and the New  $L_i^{nTh} - E_{peak,i}^{nTh,rest}$  Relation. *The Astrophysical Journal*, 2015b, 814(1), 10-35. [10.1088/0004-637X/814/1/10](https://doi.org/10.1088/0004-637X/814/1/10).

17. Huang S, Yin Y, Peng Z.-Y. Investigating the thermal component in GRB100724B. *Astrophysics and Space Science*, 2016, 361, 362-371. [10.1007/s10509-016-2937-3](https://doi.org/10.1007/s10509-016-2937-3).
18. Katz J I. Low-Frequency Spectra of Gamma-Ray Bursts. *The Astrophysical Journal*, 1994, 432, L107-L109. [10.1086/187523](https://doi.org/10.1086/187523).
19. Lundman C, Pe'er A, Ryde F. A theory of photospheric emission from relativistic, collimated outflows. *Monthly Notices of the Royal Astronomical Society*, 2013, 428, 2430-2442. [10.1093/mnras/sts219](https://doi.org/10.1093/mnras/sts219).
20. Liang E W, Dai Z G, Wu X F. The Luminosity- $E_p$  Relation within Gamma-Ray Bursts and the Implications for Fireball Models. *The Astrophysical Journal*, 2004, 606, L29-L32. [10.1086/421047](https://doi.org/10.1086/421047).
21. MacFadyen A I, Woosley S E. Collapsars: Gamma-Ray Bursts and Explosions in "Failed Supernovae". *The Astrophysical Journal*, 1999, 524, 262-289. [10.1086/307790](https://doi.org/10.1086/307790).
22. Medvedev M V. Theory of "Jitter" Radiation from Small-Scale Random Magnetic Fields and Prompt Emission from Gamma-Ray Burst Shocks. *The Astrophysical Journal*, 2000, 540, 704-714. [10.1086/309374](https://doi.org/10.1086/309374).
23. Medvedev M V. The Theory of Spectral Evolution of the Gamma-Ray Burst Prompt Emission. *The Astrophysical Journal*, 2006, 637, 869-872. [10.1086/498697](https://doi.org/10.1086/498697).
24. Meegan C A, Fishman G J, Wilson R B, Paciesas W. S, Brock M N, Horack J M, et al. Gamma-Ray Bursts. 1992, IAU Circ, 5641.
25. Meegan C, Lichti G, Bhat P N, Bissaldi E, Briggs M S, Connaughton V, et al. The Fermi Gamma-ray Burst Monitor. *The Astrophysical Journal*, 2009, 702, 791-804. [10.1088/0004-637X/702/1/791](https://doi.org/10.1088/0004-637X/702/1/791).
26. Mészáros P, Rees M J. Gamma-Ray Bursts: Multiwaveband Spectral Predictions for Blast Wave Models. *The Astrophysical Journal*, 1993, 418, L59-L62. [10.1086/187116](https://doi.org/10.1086/187116).
27. Narayan R, Kumar P. A turbulent model of gamma-ray burst variability. 2009, MNRAS, 394, L117-L120. [10.1111/j.1745-3933.2009.00624.x](https://doi.org/10.1111/j.1745-3933.2009.00624.x).
28. Paczynski B. Gamma-ray bursters at cosmological distances. *The Astrophysical Journal*, 1986, 308, L43-L46. [10.1086/184740](https://doi.org/10.1086/184740).
29. Pe'er A. Temporal Evolution of Thermal Emission from Relativistically Expanding Plasma. *The Astrophysical Journal*, 2008, 682(1), 463-473. [10.1086/588136](https://doi.org/10.1086/588136).
30. Pe'er A, Ryde F. Theoretical Implications of Thermal Emission from Gamma-Ray Bursts.
31. Peng Z. Y, Ma L, Zhao X H, Yin Y, Fang L M, Bao Y Y. The  $E_p$  Evolutionary Slope Within the Decay Phase of "Fast Rise and Exponential Decay" Gamma-Ray Burst Pulse. *The Astrophysical Journal*, 2009, 698, 417-427. [10.1088/0004-637X/698/1/417](https://doi.org/10.1088/0004-637X/698/1/417).
32. Rees M J, Mészáros P. Unsteady Outflow Models for Cosmological Gamma-Ray Bursts. *Astrophysical Journal Letters*, 1994, 430, L93-L96. [10.1086/187446](https://doi.org/10.1086/187446)
33. Rees M J, Mészáros, P. Dissipative Photosphere Models of Gamma-Ray Bursts and X-Ray Flashes. *The Astrophysical Journal*, 2005, 628, 847-852. [10.1086/430818](https://doi.org/10.1086/430818).
34. Rosswog S, Ramirez-Ruiz E, Davies M B. High-resolution calculations of merging neutron stars - III. Gamma-ray bursts. *Monthly Notices of the Royal Astronomical Society*, 2003, 345(4), 1077-1090. [10.1046/j.1365-2966.2003.07032.x](https://doi.org/10.1046/j.1365-2966.2003.07032.x)
35. Ryde F. The Cooling Behavior of Thermal Pulses in Gamma-Ray Bursts. *The Astrophysical Journal*, 2004, 614, 827-846. [10.1086/423782](https://doi.org/10.1086/423782).
36. Ryde F. Is Thermal Emission in Gamma-Ray Bursts Ubiquitous? *The Astrophysical Journal*, 2005, 625, L95-L98. [10.1086/431239](https://doi.org/10.1086/431239).

37. Ryde F, Pe'er A. Quasi-blackbody Component and Radiative Efficiency of the Prompt Emission of Gamma-ray Bursts. *The Astrophysical Journal*, 2009, 702, 1211-1229. [10.1088/0004-637X/702/2/1211](https://doi.org/10.1088/0004-637X/702/2/1211).
38. Sari R, Piran T, Narayan R. Spectra and Light Curves of Gamma-Ray Burst Afterglows. *The Astrophysical Journal*, 1998, 497, L17-L20. [10.1086/311269](https://doi.org/10.1086/311269).
39. Sironi L, Spitkovsky, A. Synthetic Spectra from Particle-In-Cell Simulations of Relativistic Collisionless Shocks. *The Astrophysical Journal*, 2009, 707, L92-L96. [10.1088/0004-637X/707/1/L92](https://doi.org/10.1088/0004-637X/707/1/L92).
40. Tavani M. A Shock Emission Model for Gamma-Ray Bursts. II. Spectral Properties. 1996, *The Astrophysical Journal*, 466, 768-778. [10.1086/177551](https://doi.org/10.1086/177551).
41. Woosley S. E. Gamma-Ray Bursts from Stellar Mass Accretion Disks around Black Holes. *The Astrophysical Journal*, 1993, 405, 273-277. [10.1086/172359](https://doi.org/10.1086/172359).
42. Wu Q W, Zou Y C, Cao X, et al. A Uniform Correlation between Synchrotron Luminosity and Doppler Factor in Gamma-Ray Bursts and Blazars: hint or similar intrinsic luminosities? *Astrophysics Journal Letter*, 2011, 740(1):1441-1458.
43. Yonetoku D, Murakami T, Nakamura T, Yamazaki R, Inoue A K, Ioka K. Gamma-Ray Burst Formation Rate Inferred from the Spectral Peak Energy-Peak Luminosity Relation. *The Astrophysical Journal*, 2004, 609, 935-951. [10.1086/421285](https://doi.org/10.1086/421285).
44. Yu H.-F, Preece R D, Greiner J, Narayana B P, Bissaldi E, Briggs M S, et al. The Fermi GBM gamma-ray burst time-resolved spectral catalog: brightest bursts in the first four years. *Astronomy & Astrophysics*, 2016, 588,135-154. [10.1051/0004-6361/201527509](https://doi.org/10.1051/0004-6361/201527509).
45. Zhang B, Mészáros P. Gamma-Ray Bursts: progress, problems & prospects. *International Journal of Modern Physics A*, 2004, 19, 2385-2472. [10.1142/S0217751X0401746X](https://doi.org/10.1142/S0217751X0401746X).
46. Zhang B, Pe'er A. Evidence of an Initially Magnetically Dominated Outflow in GRB 080916C. *The Astrophysical Journal Letters*, 2009, 700, L65-L68. [10.1088/0004-637X/700/2/L65](https://doi.org/10.1088/0004-637X/700/2/L65).
47. Zhang B, Yan H. The Internal-collision-induced Magnetic Reconnection and Turbulence (ICMART) Model of Gamma-ray Bursts. *The Astrophysical Journal*, 2011, 726-752, 90. [10.1088/0004-637X/726/2/90](https://doi.org/10.1088/0004-637X/726/2/90).
48. Zhang B. Gamma-Ray Burst Prompt Emission. *International Journal of Modern Physics D*, 2014, 23, 1430002. [10.1142/S021827181430002X](https://doi.org/10.1142/S021827181430002X).